

A New Compact CRB for Delay, Doppler and Phase Estimation - Application to GNSS SPP & RTK Performance Characterization

D. Medina^{1,✉}, L. Ortega², J. Vilà-Valls³, P. Closas⁴, F. Vincent³, E. Chaumette³

¹ Institute of Communications and Navigation, German Aerospace Center (DLR), Neustrelitz, Germany

² Telecommunications for Space and Aeronautics Lab (TéSA), Toulouse, France

³ ISAE-SUPAERO, University of Toulouse, Toulouse, France.

⁴ Dept. of Electrical and Computer Engineering, Northeastern University, Boston, MA, USA.

✉ E-mail: daniel.ariasmedina@dlr.de

ISSN 1751-8644

doi: 0000000000

www.ietdl.org

Abstract: The derivation of tight estimation lower bounds is a key tool to design and assess the performance of new estimators. In this contribution, first we derive a new compact Cramér-Rao bound (CRB) for the conditional signal model, where the deterministic parameter's vector includes a real positive amplitude and the signal phase. Then, the resulting CRB is particularized to the delay, Doppler, phase and amplitude estimation for band-limited narrowband signals, which are found in a plethora of applications, making such CRB a key tool of broad interest. This new CRB expression is particularly easy to evaluate because it only depends on the signal samples, then being straightforward to evaluate independently of the particular baseband signal considered. We exploit this CRB to properly characterize the achievable performance of satellite-based navigation systems and the so-called Real-Time Kinematics (RTK) solution. To the best of our knowledge this is the first time these techniques are theoretically characterized from the baseband delay/phase estimation processing to position computation, in terms of the CRB and maximum likelihood estimation.

1 Introduction

Time-delay estimation has been a research topic of significant interest in many fields such as radar, sonar, communications and navigation [1–6], to name a few, mainly because this drives the first stage of the receiver in order to localize and track radiating sources [7]. In addition, phase estimation is also a fundamental part in many applications, for instance, Global Navigation Satellite Systems (GNSS) precise navigation approaches rely on the exploitation of the signal phase information. Indeed, the phase measurement is linked to the wavelength which in this case is much smaller than the baseband signal resolution. This is also the case in precise GNSS remote sensing altimetry applications [8–10], where the phase must be exploited to achieve cm altimetric precision. In a broader perspective, these applications typically deal with complex circular observation vectors [11]. Within this class, an important estimation problem is the identification of the components of a noisy observation vector \mathbf{x} formed from a linear superposition of Q sources $\boldsymbol{\alpha}$ in noise \mathbf{w} [12–15],

$$\mathbf{x} = \mathbf{A}(\boldsymbol{\eta})\boldsymbol{\alpha} + \mathbf{w}, \quad \mathbf{x}, \mathbf{w} \in \mathbb{C}^N, \quad \mathbf{A}(\boldsymbol{\eta}) \in \mathbb{C}^{N \times Q}, \quad \boldsymbol{\alpha} \in \mathbb{C}^Q, \quad (1)$$

where the mixing matrix $\mathbf{A}(\boldsymbol{\eta})$ depends on an unknown deterministic parameter vector $\boldsymbol{\eta} \in \mathbb{R}^P$, with N, Q the number of samples and sources respectively. Within the framework of modern array processing [11, 15] two different signal models are considered: the conditional signal model (CSM) and the unconditional signal model [13]. We adopt the less constrained CSM framework. Finding the relationship between the baseband CSM used in GNSS and the performance of GNSS positioning techniques ignited this contribution.

1.1 From Multi-source to Single Source Estimation

The analog side of a classical GNSS receiver architecture includes a low noise amplifier (LNA), and a downconversion to an intermediate sampling frequency F_s , followed then by an analog-to-digital converter (ADC). At this stage, one works with a multi-source signal as (1), e.g., data samples from all the signal types broadcasted

by the satellites in view. Due to the similar incoming energy and the low cross-correlation among GNSS signals, the multiple signal can be easily split into single source CSMs. The estimation of single source CSM and its relation to the performance of GNSS positioning techniques is, in turn, the main focus of this work.

Despite nearly optimal properties (in the asymptotic regime, i.e., in the large sample regime [13] and/or high signal-to-noise (SNR) regime [16]) of conditional maximum likelihood estimators (CMLEs) on CSMs, these estimators suffer from a large computational cost, as they typically require solving a non-linear multi-dimensional (possibly high-dimensional) optimization problem. To circumvent this problem, several suboptimal techniques have been introduced: i) substituting the multidimensional search with a simpler one-dimension search, e.g., Capon or MUSIC methods [17], ii) restricting to a single source search, e.g., CLEAN [18] or Alternating Projection algorithms [19], or iii) exploiting the EXtended Invariance Principle (EXIP) [20], which is based on a re-parametrization of the problem that simplifies the ML criterion to be maximized. In EXIP, the efficiency property of the original ML is maintained (at least asymptotically) through a Weighted Least Square (WLS) refinement step by using a matched weighting matrix. The EXIP approach has been used in array [21] and/or radar [22] processing applications, and more recently in the context of GNSS [23].

In GNSS, the EXIP applied to the ML direct position estimation (DPE) [24, 25] leads to the widespread suboptimal two-step positioning approach, with the aim of providing position, velocity and time (PVT) estimates: i) first, the delay and Doppler for each satellite-to-receiver link are estimated independently; and then ii) delay and Doppler estimates are translated into the so-called pseudorange and pseudorange rate observations, the latter fused to obtain the user PVT thanks to a WLS minimization. In standard GNSS receivers these two steps are typically done sequentially and the use of pseudorange and pseudorange rate measurements is not directly linked to the baseband signal processing. That is, delay/Doppler estimation are an input to the WLS, and their corresponding covariances set somehow empirically, sometimes based on the satellite elevation or the estimated carrier-to-noise density (C/N_0) at the receiver [26–28]. The optimal estimation performance of the WLS stage can only

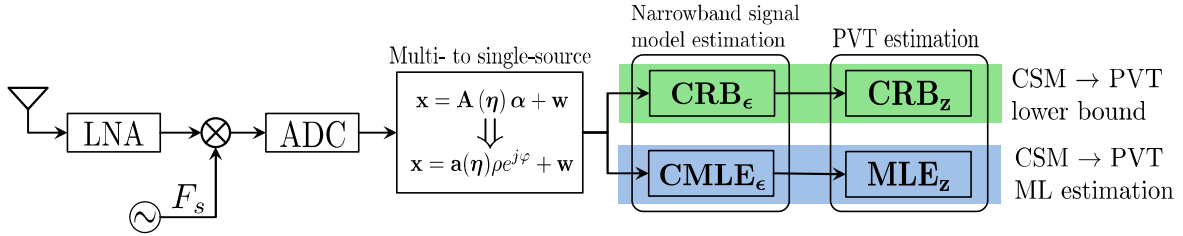


Fig. 1: Overview of the contribution for the PVT (i.e., SPP and RTK) performance characterization. From the narrowband CSM, the compact CRBs for time-delay, Doppler, phase and amplitude estimation are derived. From these signal model unknown parameters, GNSS code and phase observations are obtained and fed to the PVT estimator. Then, the CRB and the ML estimates for SPP and RTK are discussed and the overall positioning performance is addressed in direct relation to the sampling frequency and the SNR.

be assessed if the performance of the first synchronization stage is optimally determined. It is thus of the outmost importance to characterize asymptotic performance of such CMLE first step associated to the single source CSM,

$$\mathbf{x} = \mathbf{a}(\boldsymbol{\eta})\alpha + \mathbf{w}, \quad \mathbf{x}, \mathbf{w} \in \mathbb{C}^N, \quad \mathbf{a}(\boldsymbol{\eta}) \in \mathbb{C}^N, \quad \alpha \in \mathbb{C}. \quad (2a)$$

The CMLE's asymptotic performance in the mean square error (MSE) sense is accurately described by the Cramér-Rao bound (CRB). So, it is not surprising that several CRB expressions for the single source estimation problem have been derived, for finite [29–33] or infinite [34] bandwidth signals, where the starting point is often either the Slepian-Bangs formulas [35] or general theoretical CRB expressions for Gaussian observation models [15, 17, 36].

When the use of GNSS precise positioning approaches are required (i.e., in intelligent transportation systems or safety-critical applications [37]), such as the so-called Real-Time Kinematics (RTK) [38, Ch. 26] or Precise Point Positioning (PPP) techniques [38, Ch. 25], the solution involves exploiting, together with delay and Doppler, the signal phase information as well. As a consequence, with respect to (w.r.t.) the single source CSM in (2a), in addition to $\boldsymbol{\eta}$, precise positioning requires estimation of the signal amplitude and phase, and thus the following reparametrization can be used

$$\mathbf{x} = \mathbf{a}(\boldsymbol{\eta})\rho e^{j\varphi} + \mathbf{w}, \quad \mathbf{x}, \mathbf{w} \in \mathbb{C}^N, \quad \mathbf{a}(\boldsymbol{\eta}) \in \mathbb{C}^N, \quad \rho \in \mathbb{R}^+. \quad (2b)$$

To the best of our knowledge, no compact CRB formula for the joint estimation of $\boldsymbol{\epsilon}^\top = (\sigma_w^2, \rho, \varphi, \boldsymbol{\eta}^\top)$, where σ_w^2 is the power of the white noise vector \mathbf{w} (such that $\mathbf{w} \sim \mathcal{CN}(\mathbf{0}, \sigma_w^2 \mathbf{I}_N)$), seems to be available in the open literature [13–15, 17, 29–36, 39–46]. Only by assessing the performance of CMLE at the single source CSM, the stochastic modeling of PVT observables can be determined.

1.2 Contributions

- The derivation of a new compact CRB for the general CSM in (2b) is provided in Section 4. A noteworthy feature of the new compact CRB is its ease-of-use for problems where the CRBs on $\boldsymbol{\eta}$ and α (complex amplitude instead of amplitude and phase) have already been computed.
- The particularization of the compact CRB for the general CSM for the GNSS narrowband signal model is presented. Such CRB constitutes the extension of the preliminary results in [47], where a CRB for time-delay estimation under constant transmitter-to-receiver propagation delay (i.e., no Doppler effect and static scenario) was considered. In this contribution the more comprehensive case of joint delay, Doppler, phase and amplitude estimation is considered, with the corresponding CRB being derived in Section 5. Indeed the general problem is encountered in a multitude of applications, therefore a tractable CRB for this problem constitutes a key tool of broad interest. The new CRB is obtained for the standard narrowband signal model, where the Doppler effect on the band-limited baseband signal is not considered and amounts to a frequency shift.
- The CRB is expressed in terms of the signal samples, making it especially easy to use irrespective of the considered baseband signal such that the actual sample values are used.

- Leveraging recent results on the CRB for a mixture of real-and integer-valued parameter vectors [48], summarized in Section 6 for completeness, we exploit both CRBs to properly characterize the ultimate GNSS SPP and RTK performance. To the best of our knowledge this is the first time these positioning techniques are theoretically characterized from the baseband signal model in terms of the CRB and CMLE. Important findings are i) the achievable SPP performance with large GNSS bandwidth signals, and the corresponding receiver operation point which allows to reach the PVT asymptotic behavior, and ii) the impact of such GNSS signals in the RTK asymptotic behavior and the CMLE threshold region. Pictorial support for the narrowband CSM to PVT performance characterization is provided in Fig. 1.

1.3 Notation and Organization

The notation convention adopted is as follows: scalars, vectors and matrices are represented, respectively, by italic, bold lowercase and bold uppercase characters. The scalar/matrix/vector transpose and conjugate transpose are indicated by the superscripts $(\cdot)^\top$ and $(\cdot)^H$. \mathbf{I} is the identity matrix. $[\mathbf{A} \ \mathbf{B}]$ and $[\mathbf{A}]$ denote the matrix resulting from the horizontal and the vertical concatenation of \mathbf{A} and \mathbf{B} , respectively. $\text{Re}(\cdot)$ and $\text{Im}(\cdot)$ refer to the real and imaginary part. $\|\cdot\|$ describes an Euclidean norm and the norm w.r.t. \mathbf{A} is $\|\cdot\|_{\mathbf{A}} = (\cdot)^\top \mathbf{A}^{-1}(\cdot)$. $\text{tr}(\cdot)$ represents the trace operator and $\text{diag}(\cdot)$ refers to a diagonal matrix whose entries are given by (\cdot) .

The article is organized as follows. The narrowband signal model is detailed in Section 2, and both SPP and RTK are introduced in Section 3. The new CRB for the generic CSM is given in Section 4. The CRB for the joint delay, Doppler, phase and amplitude estimation for narrowband signals is derived in Section 5. The main results for the mixed real-integer parameters CRB [48] are summarized in Section 6. Finally, a complete discussion on the GNSS SPP and RTK performance is given in Section 7. Conclusion and final remarks are drawn in Section 8.

2 Standard Narrowband Signal Model

Given a generic band-limited signal $c(t)$ with bandwidth B (for instance, it can represent the so-called Pseudo-Random Noise (PRN) code in the GNSS terminology), it can be expressed in time and frequency as

$$c(t) = \sum_{n=N_1}^{N_2} c(nT_s) \text{sinc}(\pi F_s(t - nT_s)) = \\ c(f) = \left(T_s \sum_{n=N_1}^{N_2} c(nT_s) e^{-j2\pi nT_s} \right) 1_{[-\frac{B}{2}, \frac{B}{2}]}(f), \quad (3a)$$

where $F_s \geq B$, $c(nT_s)$ are the samples of $c(t)$, $N_1, N_2 \in \mathbb{Z}$, $N_1 \leq N_2$ and $=$ refers to the time-frequency pair. We consider the transmission of this band-limited signal $c(t)$ over a carrier frequency f_c (such that $\lambda_c = c/f_c$, with c the speed of light in vacuum), from a transmitter T to a receiver R. Both transmitter and receiver are in uniform linear motion: their respective positions evolve as

$\mathbf{p}_T(t) = \mathbf{p}_T + \mathbf{v}_T t$ and $\mathbf{p}_R(t) = \mathbf{p}_R + \mathbf{v}_R t$, where \mathbf{p} and \mathbf{v} represent the corresponding position and velocity vectors. In this context, we tackle the case where the propagation delay $\tau_0(t)$ due to the relative radial movement between T and R can be approximated, during the observation time, by a first order distance-velocity model

$$\begin{aligned} \|\mathbf{p}_{TR}(t)\| &\triangleq \|\mathbf{p}_T(t - \tau_0(t)) - \mathbf{p}_R(t)\| = c\tau_0(t) \simeq d + vt \\ \Rightarrow \tau_0(t) &\simeq \tau + bt, \quad \tau = \frac{d}{c}, \quad b = \frac{v}{c}, \end{aligned} \quad (3b)$$

where d is the T-to-R relative radial distance, v is the T-to-R relative radial velocity, and b is a delay drift related to the Doppler effect.

This so-called relative uniform radial movement is characterized by the time-delay (τ) due to the propagation path and the dilation ($1 - b$) induced by the Doppler effect. Under the narrowband hypothesis, i.e., $B \ll f_c$, the Doppler effect on the band-limited baseband signal $c(t)$ may be considered negligible: $c((1 - b)(t - \tau)) \approx c(t - \tau)$. In this case, for an ideal transmitter, propagation channel and receiver, the signal at the output of the receiver's Hilbert filter (I/Q demodulation, bandwidth F_s) is well approximated as [29, (2.1)][33, (3)]:

$$x(t) \triangleq x(t; \boldsymbol{\eta}) = \alpha c(t - \tau) e^{-j\omega_c b(t - \tau)} + w(t), \quad (3c)$$

$$R_w(\tau) = \sigma_w^2 \text{sinc}(\pi F_s \tau) \Rightarrow R_w(f) = \frac{\sigma_w^2}{F_s}, \quad f \in \left[-\frac{F_s}{2}, \frac{F_s}{2}\right]$$

where $\omega_c = 2\pi f_c$, $\boldsymbol{\eta}^\top = (\tau, b)$, and α is a complex amplitude which includes all the transmission budget terms. The Fourier pair $R_w(\tau) \Rightarrow R_w(f)$ is the model for the correlation function and the power spectrum density of white noise over the band F_s . If we consider the acquisition of $N' = N'_2 - N'_1 + 1$ ($N'_1 \ll N_1, N'_2 \gg N_2$) samples at $T_s = 1/F_s$, then the discrete vector signal model is given by (2a), or equivalently (2b), with

$$\mathbf{x} = \mathbf{a}(\boldsymbol{\eta}) \rho e^{j\varphi} + \mathbf{w}, \quad \rho \in \mathbb{R}^+, \quad 0 \leq \varphi \leq 2\pi, \quad (3d)$$

$$\mathbf{x}^\top = (\dots, x(n'T_s), \dots),$$

$$\mathbf{a}^\top(\boldsymbol{\eta}) = (\dots, c(n'T_s - \tau) e^{-j\omega_c b(n'T_s - \tau)}, \dots),$$

$$\mathbf{w}^\top = (\dots, w(n'T_s), \dots),$$

for $N'_1 \leq n' \leq N'_2$ (dimension N'). We also define $\mathbf{c}^\top \triangleq (\dots, c(nT_s), \dots)$, for $N_1 \leq n \leq N_2$ (dimension N). Notice that $c(t)$ can be directly a PRN code with a Binary Phase Shift Keying (BPSK) modulation where there is no subcarrier, as in the case of the GPS L1 C/A signal, or a subcarrier modulated PRN, i.e., using a Binary Offset Carrier (BOC) [49] type modulation such in the modernized GPS L1C or Galileo E1 Open Service signals. The subcarrier has a direct impact on the correlation function, therefore on the estimation performance. On top of that, the signal may have data bits or not, depending if it belongs to a data component or a pilot component.

3 GNSS SPP/RTK Problem Formulation

3.1 GNSS Baseband Signal Processing

As already stated, using the EXIP principle within the ML DPE [24] leads to the standard GNSS two-step positioning approach [23]. The first step relies on the CMLEs of delay, Doppler and phase for each individual satellite, which are expressed as

$$\hat{\boldsymbol{\eta}} = \arg \max_{\boldsymbol{\eta}} \left\{ \left| \left(\mathbf{a}^H(\boldsymbol{\eta}) \mathbf{a}(\boldsymbol{\eta}) \right)^{-1} \mathbf{a}^H(\boldsymbol{\eta}) \mathbf{x} \right|^2 \right\}, \quad (4a)$$

$$\hat{\varphi}(\hat{\boldsymbol{\eta}}) = \arg \left\{ \left(\mathbf{a}^H(\hat{\boldsymbol{\eta}}) \mathbf{a}(\hat{\boldsymbol{\eta}}) \right)^{-1} \mathbf{a}^H(\hat{\boldsymbol{\eta}}) \mathbf{x} \right\}. \quad (4b)$$

Notice that the phase CMLE is given by the argument of the cross-ambiguity function evaluated at the delay and Doppler CMLEs.

Then, if the delay-Doppler CMLE reached its asymptotic performance then so does the phase estimate.

3.2 GNSS Code and Phase Observables

From the delay and phase CMLEs introduced in Section 3.1, together with the navigation data demodulation, one constructs the so-called code and phase observables. More precisely, we are interested in the pseudorange $\hat{\varrho}_i$ and phase $\hat{\Phi}_i$ observables, which for the i -th satellite are modeled as

$$\begin{aligned} \hat{\varrho}_i &= c\hat{\tau}_i = \|\mathbf{p}_{T_i} - \mathbf{p}_R\| + c(\delta t_r - \delta t_i) \\ &\quad + c\delta t_i^{\text{iono}} + c\delta t_i^{\text{trop}} + \epsilon_{\varrho,i}, \end{aligned} \quad (5)$$

$$\begin{aligned} \hat{\Phi}_i &= \frac{\lambda_c}{2\pi} \hat{\varphi}_i = \|\mathbf{p}_{T_i} - \mathbf{p}_R\| + c(\delta t_r - \delta t_i) \\ &\quad - c\delta t_i^{\text{iono}} + c\delta t_i^{\text{trop}} + \lambda_c N_i + \epsilon_{\Phi,i}, \end{aligned} \quad (6)$$

where $\|\mathbf{p}_{T_i} - \mathbf{p}_R\| = \sqrt{(x_i - x_R)^2 + (y_i - y_R)^2 + (z_i - z_R)^2}$ is the geometrical distance between the receiver and the i -th satellite; $\mathbf{p}_R^\top = [x_R, y_R, z_R]$ and $\mathbf{p}_{T_i}^\top = [x_i, y_i, z_i]$ are the position coordinates of the receiver and the i -th satellite, respectively; the R-to-T unitary line-of-sight vector is $\mathbf{u}_i(\mathbf{p}_R) = \frac{\mathbf{p}_{T_i} - \mathbf{p}_R}{\|\mathbf{p}_{T_i} - \mathbf{p}_R\|}$; δt_r and δt_i are the receiver and satellite clock offsets w.r.t. the GNSS time. δt_i^{iono} and δt_i^{trop} are the ionospheric and tropospheric delays, respectively. Since in the asymptotic region, i.e., at high SNR, the CMLE becomes unbiased, efficient and Gaussian distributed [16], $\epsilon_{\varrho,i}$ and $\epsilon_{\Phi,i}$ are zero-mean white Gaussian noise terms. λ_c is the carrier wavelength and N_i is an ambiguous term related to the (unknown) number of phase cycles. The latter has a fractional part B_i which depends on the initial phase of the i -th satellite clock, a fractional part B_r due to initial phase at the receiver, and an integer part $N_{\text{int},i}$ which is related to the satellite to receiver distance, then $N_i = B_i + B_r + N_{\text{int},i}$. Notice that the variance of $\epsilon_{\varrho,i}$ and $\epsilon_{\Phi,i}$ is driven by the performance of $\hat{\boldsymbol{\eta}}$ and $\hat{\varphi}(\hat{\boldsymbol{\eta}})$, respectively.

3.3 GNSS Code-based SPP PVT

Let us consider M satellites being tracked, then the set of M pseudoranges is $\mathbf{y}_\varrho^\top = [\hat{\varrho}_1, \dots, \hat{\varrho}_M]$. The unknown parameters are gathered in vector $\boldsymbol{\gamma}^\top = [\mathbf{p}_R^\top, c\delta t_r]$, which includes the 3D receiver position and receiver clock offset. From $\epsilon_{\varrho,i}$ we define the complete noise term as $\mathbf{n}_\varrho^\top = [\epsilon_{\varrho,1}, \dots, \epsilon_{\varrho,M}]$, with covariance $\mathbf{C}_{\mathbf{n},\varrho}$. The nonlinear observation model is then expressed as $\mathbf{y}_\varrho = \mathbf{h}(\boldsymbol{\gamma}) + \mathbf{n}_\varrho$.

The standard way to solve this problem is to consider an initial position \mathbf{p}^0 (i.e., typically equal to $\mathbf{0}$) and then linearize the observation function around this point, $\|\mathbf{p}_{T_i} - \mathbf{p}_R\| \approx \|\mathbf{p}_{T_i} - \mathbf{p}^0\| - \mathbf{u}_i(\mathbf{p}^0)\delta_p$, with $\delta_p = \mathbf{p}_R - \mathbf{p}^0$. Additionally, from the navigation message we have (an estimate of) δt_i , δt_i^{iono} and δt_i^{trop} , then we can build a new observation vector, $\tilde{\mathbf{y}}_\varrho$, whose elements are corrected accordingly. For instance, the i -th element is modeled as

$$\tilde{y}_i = \hat{\varrho}_i + c\delta t_i - c\delta t_i^{\text{iono}} - c\delta t_i^{\text{trop}} - \|\mathbf{p}_{T_i} - \mathbf{p}^0\|, \quad (7a)$$

for $1 \leq i \leq M$. Therefore, the nonlinear measurement function is approximated by the following linearized measurement matrix

$$\widehat{\mathbf{H}}(\mathbf{p}^0) = \begin{bmatrix} -\mathbf{u}_1^\top(\mathbf{p}^0) & 1 \\ \vdots & \vdots \\ -\mathbf{u}_M^\top(\mathbf{p}^0) & 1 \end{bmatrix}. \quad (7b)$$

The observation model is approximated as $\tilde{\mathbf{y}}_\varrho \approx \widehat{\mathbf{H}}(\mathbf{p}^0)\delta + \mathbf{n}_\varrho$ with $\delta = [\delta_p^\top \ c\delta t_r]^\top$, for which the WLS solution is

$$\begin{aligned} \hat{\delta}_{WLS} &= \arg \min_{\delta} \{ \|\tilde{\mathbf{y}}_\varrho - \widehat{\mathbf{H}}(\mathbf{p}^0)\delta\|_{\mathbf{W}}^2 \} \\ &= \left(\widehat{\mathbf{H}}^\top(\mathbf{p}^0) \mathbf{W} \widehat{\mathbf{H}}(\mathbf{p}^0) \right)^{-1} \widehat{\mathbf{H}}^\top(\mathbf{p}^0) \mathbf{W} \tilde{\mathbf{y}}_\varrho, \end{aligned} \quad (7c)$$

which can be easily reformulated as an iterative WLS (i.e., iterate until the solution between two consecutive iterations - that is, j and $j + 1$ - is smaller than a predefined threshold ζ , $\|\mathbf{p}^{j+1} - \mathbf{p}^j\| < \zeta$). The weighting matrix \mathbf{W} is related to the measurement error. If errors among measurements are uncorrelated \mathbf{W} is diagonal. Considering that the corrections obtained from the navigation message are perfect, then the WLS is the best linear unbiased estimator (BLUE) if $\mathbf{W} = \mathbf{C}_{n,\varrho}^{-1}$.

3.4 GNSS Code/Phase-based RTK Positioning

RTK is a differential positioning approach for which the location of the receiver of interest is referred to that of a nearby base station. Due to the proximity between the target and base receivers, these are influenced by the same propagation errors. Thus, code and carrier double-differencing (*i.e.*, subtracting the measurements from the rover receiver w.r.t. the base station and a pivot satellite) leads to the elimination of nuisance parameters (*e.g.*, atmospheric delays, clock and instrumental errors) and phase observations influenced by an integer number of ambiguities. The problem of mixed integer and real parameter estimation has been extensively studied within the GNSS community [50–52] and its resolution typically combines a WLS and an Integer LS (ILS).

Let us consider $M + 1$ satellites being tracked simultaneously at the base and rover receivers. Subscripts 0 and superscript B are used to refer to the pivot satellite and the base station, respectively. Superscript R refers to quantities from the rover receiver. Code and carrier double differences are built as follows

$$\hat{\varrho}_{i,0}^{R,B} = \hat{\varrho}_i^R - \hat{\varrho}_i^B - (\hat{\varrho}_0^R - \hat{\varrho}_0^B) \quad (8a)$$

$$\hat{\Phi}_{i,0}^{R,B} = \hat{\Phi}_i^R - \hat{\Phi}_i^B - (\hat{\Phi}_0^R - \hat{\Phi}_0^B), \quad (8b)$$

and the vectors stacking the M double-difference code and carrier observations are defined as $\mathbf{y}_\varrho^\top = [\hat{\varrho}_{1,0}^{R,B}, \dots, \hat{\varrho}_{M,0}^{R,B}]$ and $\mathbf{y}_\Phi^\top = [\hat{\Phi}_{1,0}^{R,B}, \dots, \hat{\Phi}_{M,0}^{R,B}]$, respectively. Under the assumption that the unitary steering vector to the satellites is shared across the base and rover receivers, the RTK observation model is generally presented in the following linearized form

$$\mathbf{y} = \mathbf{D}\mathbf{z} + \mathbf{n}_{\Phi,\varrho}, \quad \mathbf{y} = \begin{bmatrix} \mathbf{y}_\Phi \\ \mathbf{y}_\varrho \end{bmatrix}, \quad \mathbf{z} = \begin{bmatrix} \mathbf{b} \\ \mathbf{a} \end{bmatrix}, \quad (9a)$$

$$\mathbf{D} = \begin{bmatrix} \mathbf{B} & \mathbf{A} \\ \mathbf{B} & \mathbf{0} \end{bmatrix}, \quad \mathbf{B} = \begin{bmatrix} -(\mathbf{u}_1(\mathbf{p}_B) - \mathbf{u}_0(\mathbf{p}_B))^\top \\ \vdots \\ -(\mathbf{u}_M(\mathbf{p}_B) - \mathbf{u}_0(\mathbf{p}_B))^\top \end{bmatrix}, \quad \mathbf{A} = \lambda_c \mathbf{I}, \quad (9b)$$

with the noise terms

$$\mathbf{n}_{\Phi,\varrho} = \begin{bmatrix} \mathbf{n}_\Phi \\ \mathbf{n}_\varrho \end{bmatrix}, \quad \mathbf{C}_n = \begin{bmatrix} \mathbf{C}_{\mathbf{n}_\Phi} & \mathbf{C}_{\mathbf{n}_\Phi, \mathbf{n}_\varrho} \\ \mathbf{C}_{\mathbf{n}_\Phi, \mathbf{n}_\varrho}^\top & \mathbf{C}_{\mathbf{n}_\varrho} \end{bmatrix}, \quad (9c)$$

$$\mathbf{C}_{\{\Phi,\varrho\}} = [-\mathbf{1}_{M,1} \mathbf{I}] \begin{bmatrix} \sigma_{\{\Phi,\varrho\}0}^2 & 0 \\ 0 & \ddots & \sigma_{\{\Phi,\varrho\}M}^2 \end{bmatrix} [-\mathbf{1}_{M,1} \mathbf{I}]^\top \quad (9d)$$

where \mathbf{z} in (9a) is the set of unknown parameters constituted by the baseline vector between rover and base station, $\mathbf{b} = \mathbf{p}_R - \mathbf{p}_B$, and the vector of double difference integer ambiguities \mathbf{a} . Notice that the contribution of ambiguity fractional parts B_i and B_r in (6) disappears due to double-differencing. The covariance matrix \mathbf{C}_n comprises the covariance matrices of the double difference phase and code observations, as well as the cross-correlations between them. The individual variances of the phase and carrier observations

$\sigma_{\{\Phi,\varrho\}i}^2$ for $i = 0, \dots, M$, are conditioned to the signal used and can be accurately derived from the CRB in Section 5.

RTK positioning can be cast as a minimization problem over mixed integer-real parameters, whose argument is the **integer double difference ambiguities \mathbf{a}** and the **baseline vector \mathbf{b}** , as

$$\underbrace{\begin{bmatrix} \hat{\mathbf{b}} \\ \hat{\mathbf{a}} \end{bmatrix}}_{\hat{\mathbf{z}}} = \arg \min_{\substack{\mathbf{b} \in \mathbb{R}^3 \\ \mathbf{a} \in \mathbb{Z}^M}} \left\| \mathbf{y} - \mathbf{D} \begin{bmatrix} \mathbf{b} \\ \mathbf{a} \end{bmatrix} \right\|_{\mathbf{C}_n}^2. \quad (10)$$

A closed-form solution to (10) is not known, due to the integer nature of the ambiguities. Instead, a three-step decomposition of the problem is typically considered [50], and the resulting minimization problems are sequentially resolved as [53]

$$\min_{\substack{\mathbf{b} \in \mathbb{R}^3 \\ \mathbf{a} \in \mathbb{Z}^M}} \left\| \mathbf{y} - \mathbf{D} \begin{bmatrix} \mathbf{b} \\ \mathbf{a} \end{bmatrix} \right\|_{\mathbf{C}_n}^2 = \left\| \mathbf{y} - \mathbf{D} \begin{bmatrix} \bar{\mathbf{b}} \\ \bar{\mathbf{a}} \end{bmatrix} \right\|_{\mathbf{C}_n}^2 \quad (11a)$$

$$+ \min_{\mathbf{a} \in \mathbb{Z}^M} \|\bar{\mathbf{a}} - \mathbf{a}\|_{\mathbf{C}_{\bar{\mathbf{a}}}}^2 \quad (11b)$$

$$+ \min_{\mathbf{b} \in \mathbb{R}^3} \|\bar{\mathbf{b}} - \mathbf{b}\|_{\mathbf{C}_{\bar{\mathbf{b}}|\mathbf{a}}}^2, \quad (11c)$$

where the first term (11a) corresponds to the WLS solution where the ambiguities are treated as real numbers (instead of integer quantities). The output of this estimate $\bar{\mathbf{z}}^\top = [\bar{\mathbf{b}}^\top, \bar{\mathbf{a}}^\top]$ is referred to as *float solution* and its associated covariance matrix is

$$\mathbf{C}_{\bar{\mathbf{z}}} = \begin{bmatrix} \mathbf{C}_{\bar{\mathbf{b}}} & \mathbf{C}_{\bar{\mathbf{b}}, \bar{\mathbf{a}}} \\ \mathbf{C}_{\bar{\mathbf{a}}, \bar{\mathbf{b}}} & \mathbf{C}_{\bar{\mathbf{a}}} \end{bmatrix}.$$

The second term (11b) in the decomposition corresponds to the ILS, for which an integer solution $\bar{\mathbf{a}}$ for the ambiguities \mathbf{a} is found. A profound discussion on estimators for integer estimation problems can be found in [38, Ch. 23] and therein. Finally, the third term (11c) is the *fix solution*, consisting on enhancing the localization estimates upon the estimated integer ambiguities, resolved applying a WLS adjustment

$$\mathbf{b} = \bar{\mathbf{b}} - \mathbf{C}_{\bar{\mathbf{b}}, \bar{\mathbf{a}}} \mathbf{C}_{\bar{\mathbf{a}}}^{-1} (\bar{\mathbf{a}} - \check{\mathbf{a}}). \quad (12)$$

The improvement in the positioning accuracy is due to constraining the real ambiguities to integer values. An important remark is that the fixed solution will be biased whenever the estimated integer ambiguities do not match the true ones. The precision of the solution improves only when the correct ambiguities are correctly found [54].

4 A Compact CRB for the Single Source CSM

First, we provide new results on the CRB for the general CSM in (2b), which can be reparameterized as

$$\mathbf{x} = \mathbf{a}'(\boldsymbol{\theta}) \rho + \mathbf{n}, \quad \mathbf{a}'(\boldsymbol{\theta}) = \mathbf{a}(\boldsymbol{\eta}) e^{j\varphi}, \quad \boldsymbol{\theta}^\top = (\varphi, \boldsymbol{\eta}^\top), \quad (13)$$

and we recall that $\boldsymbol{\epsilon}^\top = (\sigma_n^2, \rho, \varphi, \boldsymbol{\eta}^\top)$ is to be estimated. The corresponding CRB for the estimation of $\boldsymbol{\epsilon}$ is given by*

$$\text{CRB}_\rho = \frac{\sigma_n^2}{2 \|\mathbf{a}(\boldsymbol{\eta})\|^2} + \rho^2 \frac{\text{Re} \left\{ \mathbf{a}^H(\boldsymbol{\eta}) \frac{\partial \mathbf{a}(\boldsymbol{\eta})}{\partial \boldsymbol{\eta}} \right\} \text{CRB}_\eta \text{Re} \left\{ \mathbf{a}^H(\boldsymbol{\eta}) \frac{\partial \mathbf{a}(\boldsymbol{\eta})}{\partial \boldsymbol{\eta}^\top} \right\}^\top}{\|\mathbf{a}(\boldsymbol{\eta})\|^4}, \quad (14a)$$

*Let $S = \text{span}(\mathbf{A})$, with \mathbf{A} a matrix, be the linear span of the set of its column vectors, S^\perp the orthogonal complement of the subspace S , $\boldsymbol{\Pi}_\mathbf{A} = \mathbf{A}(\mathbf{A}^H \mathbf{A}) \mathbf{A}^H$ the orthogonal projection over S , and $\boldsymbol{\Pi}_\mathbf{A}^\perp = \mathbf{I} - \boldsymbol{\Pi}_\mathbf{A}$.

$$CRB_{\sigma_n^2} = \frac{1}{N} (\sigma_n^2)^2, \quad (14b)$$

$$\mathbf{CRB}_{\boldsymbol{\theta}} = \begin{bmatrix} CRB_{\varphi} & \mathbf{CRB}_{\eta, \varphi}^\top \\ \mathbf{CRB}_{\eta, \varphi} & \mathbf{CRB}_{\eta} \end{bmatrix}, \quad (14c)$$

where the different terms in $\mathbf{CRB}_{\boldsymbol{\theta}}$ are computed as

$$\mathbf{CRB}_{\eta} = \frac{\sigma_n^2}{2\rho^2} \operatorname{Re} \left\{ \left(\frac{\partial \mathbf{a}(\boldsymbol{\eta})}{\partial \boldsymbol{\eta}^\top} \right)^H \mathbf{\Pi}_{\mathbf{a}(\boldsymbol{\eta})}^\perp \frac{\partial \mathbf{a}(\boldsymbol{\eta})}{\partial \boldsymbol{\eta}^\top} \right\}^{-1}, \quad (14d)$$

$$CRB_{\varphi} = \frac{\sigma_n^2}{2\rho^2} \frac{1}{\|\mathbf{a}(\boldsymbol{\eta})\|^2} \quad (14e)$$

$$+ \frac{\operatorname{Im} \left\{ \mathbf{a}^H(\boldsymbol{\eta}) \frac{\partial \mathbf{a}(\boldsymbol{\eta})}{\partial \boldsymbol{\eta}^\top} \right\} \mathbf{CRB}_{\eta} \operatorname{Im} \left\{ \mathbf{a}^H(\boldsymbol{\eta}) \frac{\partial \mathbf{a}(\boldsymbol{\eta})}{\partial \boldsymbol{\eta}^\top} \right\}^\top}{\|\mathbf{a}(\boldsymbol{\eta})\|^4},$$

$$\mathbf{CRB}_{\eta, \varphi} = -\mathbf{CRB}_{\eta} \frac{\operatorname{Im} \left\{ \mathbf{a}^H(\boldsymbol{\eta}) \frac{\partial \mathbf{a}(\boldsymbol{\eta})}{\partial \boldsymbol{\eta}^\top} \right\}^\top}{\|\mathbf{a}(\boldsymbol{\eta})\|^2}. \quad (14f)$$

Proof: see Appendix 10.

Surprisingly, to the best of our knowledge, the compact CRB formulas (14a)-(14f) for the joint estimation of $\boldsymbol{\epsilon}^\top = (\sigma_n^2, \rho, \varphi, \boldsymbol{\eta}^\top)$ do not seem to have been released in the open literature. A noteworthy feature of this compact CRB is its ease-of-use for problems where the CRBs on $\boldsymbol{\eta}$ and α (the complex amplitude instead of amplitude and phase) have already been computed. Indeed, since $\mathbf{a}^H(\boldsymbol{\eta}) \frac{\partial \mathbf{a}(\boldsymbol{\eta})}{\partial \boldsymbol{\eta}^\top}$ naturally appears to compute $\left(\frac{\partial \mathbf{a}(\boldsymbol{\eta})}{\partial \boldsymbol{\eta}^\top} \right)^H \mathbf{\Pi}_{\mathbf{a}(\boldsymbol{\eta})}^\perp \frac{\partial \mathbf{a}(\boldsymbol{\eta})}{\partial \boldsymbol{\eta}^\top}$ in (14d), the CRB for these problems can be readily updated in order to incorporate (14e)-(14a). A use case is shown in Appendix 10.

5 Narrowband Signal Model Delay, Doppler, Phase and Amplitude Estimation CRB

The SNR at the output of the CMLE is defined as

$$\text{SNR}_{\text{out}} = \frac{|\alpha|^2 \mathbb{E}}{\left(\frac{\sigma_n^2}{F_s} \right)} = \frac{|\alpha|^2 \mathbf{c}^H \mathbf{c}}{\sigma_n^2}, \quad \mathbb{E} = \frac{\mathbf{c}^H \mathbf{c}}{F_s},$$

and using the results in Section 4, the CRB for the estimation of $\boldsymbol{\epsilon}^\top = (\sigma_n^2, \rho, \varphi, \boldsymbol{\eta}^\top)$ considering the model in (3d) is

$$\mathbf{CRB}_{\eta} = \frac{1}{2\text{SNR}_{\text{out}}} \boldsymbol{\Delta}_{\eta}^{-1}, \quad (15a)$$

$$[\boldsymbol{\Delta}_{\eta}]_{1,1} = F_s^2 \left(\frac{\mathbf{c}^H \mathbf{V} \mathbf{c}}{\mathbf{c}^H \mathbf{c}} - \left| \frac{\mathbf{c}^H \boldsymbol{\Lambda} \mathbf{c}}{\mathbf{c}^H \mathbf{c}} \right|^2 \right)$$

$$[\boldsymbol{\Delta}_{\eta}]_{2,2} = \frac{\omega_c^2}{F_s^2} \left(\frac{\mathbf{c}^H \mathbf{D}^2 \mathbf{c}}{\mathbf{c}^H \mathbf{c}} - \left(\frac{\mathbf{c}^H \mathbf{D} \mathbf{c}}{\mathbf{c}^H \mathbf{c}} \right)^2 \right)$$

$$[\boldsymbol{\Delta}_{\eta}]_{1,2} = [\boldsymbol{\Delta}_{\eta}]_{2,1} = \omega_c \operatorname{Im} \left\{ \frac{\mathbf{c}^H \mathbf{D} \boldsymbol{\Lambda} \mathbf{c}}{\mathbf{c}^H \mathbf{c}} - \frac{\mathbf{c}^H \mathbf{D} \mathbf{c}}{\mathbf{c}^H \mathbf{c}} \frac{\mathbf{c}^H \boldsymbol{\Lambda} \mathbf{c}}{\mathbf{c}^H \mathbf{c}} \right\}$$

$$CRB_{\varphi} = \frac{1}{2\text{SNR}_{\text{out}}} + \left(F_s \operatorname{Im} \left\{ \frac{\mathbf{c}^H \boldsymbol{\Lambda} \mathbf{c}}{\mathbf{c}^H \mathbf{c}} \right\} - b\omega_c \right)^\top$$

$$\times \mathbf{CRB}_{\eta} \left(F_s \operatorname{Im} \left\{ \frac{\mathbf{c}^H \boldsymbol{\Lambda} \mathbf{c}}{\mathbf{c}^H \mathbf{c}} \right\} - b\omega_c \right), \quad (15b)$$

$$\mathbf{CRB}_{\eta, \varphi} = \mathbf{CRB}_{\eta} \left(\frac{F_s \operatorname{Im} \left\{ \frac{\mathbf{c}^H \boldsymbol{\Lambda} \mathbf{c}}{\mathbf{c}^H \mathbf{c}} \right\} - b\omega_c}{\frac{\omega_c}{F_s} \frac{\mathbf{c}^H \mathbf{D} \mathbf{c}}{\mathbf{c}^H \mathbf{c}}} \right), \quad (15c)$$

$$CRB_{\rho} = \frac{1}{2 \mathbb{E} F_s} \quad (15d)$$

$$+ \rho^2 F_s^2 \left(\operatorname{Re} \left\{ \frac{\mathbf{c}^H \boldsymbol{\Lambda} \mathbf{c}}{\mathbf{c}^H \mathbf{c}} \right\} \right)^\top \mathbf{CRB}_{\eta} \left(\operatorname{Re} \left\{ \frac{\mathbf{c}^H \boldsymbol{\Lambda} \mathbf{c}}{\mathbf{c}^H \mathbf{c}} \right\} \right),$$

$$CRB_{\sigma_n^2} = \frac{1}{N} (\sigma_n^2)^2, \quad (15e)$$

with \mathbf{D} , $\boldsymbol{\Lambda}$ and \mathbf{V} defined as

$$\mathbf{D} = \operatorname{diag} ([N_1, N_1 + 1, \dots, N_2 - 1, N_2]), \quad (16a)$$

$$(\mathbf{V})_{n,n'} = \begin{cases} n' \neq n : (-1)^{|n-n'|} \frac{2}{(n-n')^2}, \\ n' = n : \frac{\pi^2}{3} \end{cases}, \quad (16b)$$

$$(\boldsymbol{\Lambda})_{n,n'} = \begin{cases} n' \neq n : \frac{(-1)^{|n-n'|}}{(n-n')}, \\ n' = n : 0 \end{cases}, \quad (16c)$$

Proof: see Appendix 11.

6 CRB for the CSM with a Mixture of Real- and Integer-valued Parameter Vectors

In this Section we summarize the main results in [48] for the mixed real-integer parameters CRB in the linear regression problem, that is, the Gaussian CSM. These results are fundamental to characterize the second step in the GNSS RTK processing. Let's consider again the Gaussian linear observation model (9a), $\mathbf{y} \sim \mathcal{N}(\mathbf{D}\mathbf{z}, \mathbf{C}_n)$, where $\mathbf{b} \in \mathbb{R}^{K_b}$, $\mathbf{a} \in \mathbb{Z}^M$, $K_b + M = K$. The CRB in this case is

$$\mathbf{CRB}_{\mathbf{z}|\mathbf{z}} (\mathbf{z}^0) = \boldsymbol{\Lambda}_{\mathbf{z}} (\mathbf{z}^0) \bar{\mathbf{F}} (\mathbf{z}^0)^{-1} \boldsymbol{\Lambda}_{\boldsymbol{\theta}}^\top (\mathbf{z}^0), \quad (17a)$$

$$\bar{\mathbf{F}} (\mathbf{z}^0) = \begin{bmatrix} \mathbf{F}_{\mathbf{b}|\mathbf{z}} (\mathbf{z}^0) & \mathbf{H} (\mathbf{z}^0) \\ \mathbf{H} (\mathbf{z}^0)^\top & \mathbf{MS}_{\mathbf{a}|\mathbf{z}} (\mathbf{z}^0) \end{bmatrix},$$

$$\boldsymbol{\Lambda}_{\mathbf{z}} (\mathbf{z}^0) = [\mathbf{i}_1 \dots \mathbf{i}_{K_b} \mathbf{i}_{K_b+1} - \mathbf{i}_{K_b+1} \dots \mathbf{i}_K - \mathbf{i}_K],$$

with \mathbf{i}_k is the k th column of the identity matrix \mathbf{I}_K , and \mathbf{z}^0 a selected value of the parameter vector \mathbf{z} . The terms of the CRB are given by

$$\mathbf{F}_{\mathbf{b}|\mathbf{z}} (\mathbf{z}^0) = \begin{bmatrix} \mathbf{B} \\ \mathbf{B} \end{bmatrix}^\top \mathbf{C}_n^{-1} \begin{bmatrix} \mathbf{B} \\ \mathbf{B} \end{bmatrix}, \quad (17b)$$

$$\mathbf{H} (\mathbf{z}^0) = [\mathbf{B}^\top \mathbf{B}^\top] \mathbf{C}_n^{-1} \mathbf{D} [\mathbf{i}_{K_b+1} - \mathbf{i}_{K_b+1} \dots \mathbf{i}_K - \mathbf{i}_K], \quad (17c)$$

$$\mathbf{MS}_{\mathbf{a}|\mathbf{z}} (\mathbf{z}^0), \text{ for } 1 \leq i, j \leq 2M \Rightarrow [\mathbf{MS}_{\mathbf{a}|\mathbf{z}} (\mathbf{z}^0)]_{i,j} = e^{(\mathbf{z}^0 - \mathbf{z}^i - \mathbf{z}^j)^\top \mathbf{D}^\top \mathbf{C}_n^{-1} \mathbf{D} \mathbf{z}^0 + (\mathbf{z}^i)^\top \mathbf{D}^\top \mathbf{C}_n^{-1} \mathbf{D} (\mathbf{z}^j)} - 1, \quad (17d)$$

where $\mathbf{z}^l = \mathbf{z}^0 + (-1)^{l-1} \mathbf{i}_{K_b + \lfloor \frac{l+1}{2} \rfloor}$, $l = \{i, j\}$.

It is worth noting that relaxing the condition on the integer-valued part of the parameters' vector, and assuming that both parameters are real-valued, $\mathbf{b} \in \mathbb{R}^{K_b}$, $\mathbf{a} \in \mathbb{R}^M$, then the standard CRB (i.e., so-called CRB_{real} in the following Section 7) is given by the inverse of the following FIM,

$$\mathbf{F}_{\mathbf{z}|\mathbf{z}} (\mathbf{z}^0) = \mathbf{D}^\top \mathbf{C}_n^{-1} \mathbf{D}, \quad (18)$$

which using the appropriate matrices is the SPP second step CRB.

Furthermore, since $\check{\mathbf{a}}$ and $\check{\mathbf{b}}$ (i.e., see (12)) are uniformly unbiased estimates of \mathbf{a} and \mathbf{b} [38, Ch. 23], $\text{CRB}_{\mathbf{b}|\mathbf{z}}$ is a relevant lower bound for the vector of estimates $\check{\mathbf{z}}^\top = (\check{\mathbf{b}}^\top, \check{\mathbf{a}}^\top)$, where \mathbf{b} can be regarded as the parameter vector of interest and \mathbf{a} a so-called nuisance parameter vector. Since it is well known that adding unknown parameters leads to an equal or higher CRB, then [48]

$$\mathbf{C}_{\check{\mathbf{b}}} \geq \text{CRB}_{\mathbf{b}|\mathbf{z}}(\mathbf{z}^0) \geq \text{CRB}_{\mathbf{b}|\mathbf{b}}(\mathbf{b}^0) = \mathbf{F}_{\mathbf{b}|\mathbf{z}}^{-1}(\mathbf{z}^0), \quad (19a)$$

where $\mathbf{C}_{\check{\mathbf{b}}}$ denotes the covariance matrix of $\check{\mathbf{b}}$. In addition, from [38, Ch. 23], asymptotically at high SNR, i.e., as $\text{tr}(\mathbf{C}_n)$ tends to 0,

$$\lim_{\text{tr}(\mathbf{C}_n) \rightarrow 0} \mathbf{C}_{\check{\mathbf{b}}} = \mathbf{F}_{\mathbf{b}|\mathbf{z}}^{-1}(\mathbf{z}^0), \quad (19b)$$

which proves that $\check{\mathbf{b}}$ is asymptotically efficient. Since the convergence to $\text{CRB}_{\mathbf{b}|\mathbf{b}}$ is the desired behavior of the fixed-solution $\check{\mathbf{b}}$, it is then of great importance, from an operational point of view, to assess the SNR threshold where the total MSE, i.e., $\text{tr}(\mathbf{C}_{\check{\mathbf{b}}})$, departs from $\text{tr}(\mathbf{F}_{\mathbf{b}|\mathbf{z}}^{-1}(\mathbf{z}^0))$, so-called CRB_{real/integer} in the following.

7 Simulation Results and Discussion

This section addresses the positioning performance of SPP and RTK in direct relation to the GNSS receiver effectiveness at estimating the unknown parameters of the GNSS narrowband signal. Thus, the experimentation comprises two elements: *i*) the CRB and associated CMLE for the unknown delay and phase signal parameters, which in turn determines the noise levels on the code and carrier pseudorange observations; *ii*) the CRB and MLE for SPP and RTK positioning techniques, given the previously assessed performance of the receiver at the narrowband signal. For such purpose a variety of GNSS signals are studied, considering different sampling frequencies and receiver operating points. Notice that the results in this Section are given w.r.t. the SNR_{out} , that is, the SNR at the output of the CMLE matched filter, which is linked to the C/N_0 (i.e., a typical GNSS operation point indicator) as

$$\text{SNR}_{\text{out}} = \frac{F_s \alpha^2 \mathbf{c}^H \mathbf{c}}{\sigma_n^2} = \frac{C}{N_0} T_{\text{PRN}} L_c, \quad (20)$$

where T_{PRN} is the single code duration and L_c is the number of codes, therefore, $T_I = T_{\text{PRN}} \times L_c$ is the coherent integration time. The color/symbol notation followed throughout the section is summarized in Fig. 2.

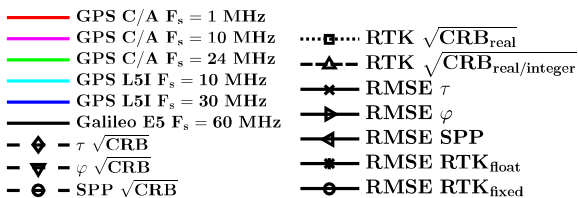


Fig. 2: Signals, CRBs and CMLEs colors and symbols.

7.1 Some Representative GNSS Signals Characteristics

In this contribution we are interested in the possible gain provided by fast codes, i.e., large bandwidths or equivalently narrow correlation functions. For that reason, GPS L1C, GPS L2, Galileo E1 Open Service or Galileo E6 signals are not considered. The GPS L1 C/A signal is considered as the benchmark. GPS L5 and Galileo E5 are representative large bandwidth signals for both systems. A brief summary of the signals' characteristics follows:

- GPS L1 C/A signal: the L1 coarse acquisition (C/A) code is the legacy GPS signal, with a navigation message at 50 bits/s, a PRN Gold sequence of 1023 chips with $T_{\text{PRN}} = 1$ ms, that is, a chip rate of 1.023 MHz, transmitted at $f_c = 1575.42$ MHz and which uses a BPSK subcarrier modulation (i.e. BPSK(1)) [55].

- GPS L5: the L5 signal, transmitted at $f_c = 1176.45$ MHz uses a BPSK(10) modulation, that is, a chip rate 10 times faster than the L1 C/A signal, 10.23 MHz. The data component (i.e., L5-I) transmits a navigation message at 100 bits/s [56].

- Galileo E5 signal: this signal has four signal components (i.e., E5A-I, E5A-Q, E5B-I and E5B-Q, I for in-phase data components and Q for quadrature pilot components, each one BPSK(10) modulated) and is allocated in two different frequency sub-bands, denoted as E5A ($f_c = 1176.45$ MHz) and E5B ($f_c = 1207.14$ MHz). The E5A-I and E5B-I data components transmit navigation messages at 50 bits/s and 250 bits/s, and their PRNs last 20 ms and 4 ms, respectively. The complete Galileo E5 signal is constructed as an AltBOC(15,10) modulated signal, i.e., the combination of the four BPSK(10) components [57].

A summary of the different GNSS signals' main characteristics is given in Table 1. The autocorrelation function (ACF) for the different signals in Table 1 is shown in Fig. 3, where the impact of the large signal bandwidth can be observed as a narrower peak.

Table 1 GPS and Galileo signals characteristics.

ACF peak refers to the first zero-crossing of the ACF, $T_{\text{PRN}} = 1$ ms.

Signal	Modulation	T_{bit}	ACF Peak
GPS L1 C/A	BPSK(1)	20 ms	$\pm 1.023\mu\text{s}$
GPS L5-I	BPSK(10)	10 ms	$\pm 0.1023\mu\text{s}$
Galileo E5	AltBOC(15,10)	4 ms	$\pm 0.0174\mu\text{s}$

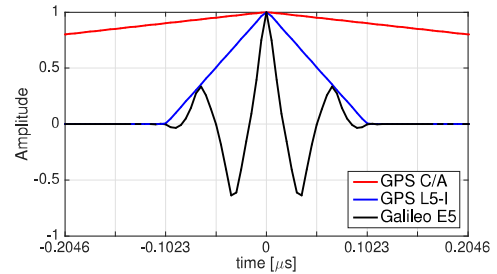


Fig. 3: GPS L1 C/A, GPS L5-I and Galileo E5 ACFs.

7.2 First Step: Delay and Phase CRB/CMLE Results

7.2.1 Delay Estimation:

The main time-delay CRB and CMLE results for the different signals considered in this article (see Table 1) are summarized in Fig. 4. First, notice that the CMLE asymptotic region threshold (i.e., the operation point where the MLE starts to rapidly deviate from the CRB) is around $\text{SNR}_{\text{out}} = 15$ dB. From (20), taking into account that $T_{\text{PRN}} = 1$ ms for all the signals considered, this threshold corresponds to a $C/N_0 = 45$ dB-Hz using 1 code ($T_I = 1$ ms), $C/N_0 = 39$ dB-Hz for 4 coherently integrated codes ($T_I = 4$ ms), $C/N_0 = 35$ dB-Hz with 10 coherently integrated codes ($T_I = 10$ ms) and $C/N_0 = 32$ dB-Hz for the L1 C/A T_{bit} limit of 20 codes ($T_I = 20$ ms).

Let's first compare the time-delay estimation results for the GPS L1 C/A signal considering different $F_s = 1, 10$ and 24 MHz, the latter being the full signal bandwidth. For a receiver operation point $\text{SNR}_{\text{out}} = 25$ dB, which for a nominal $C/N_0 = 45$ dB-Hz corresponds to a standard $T_I = 10$ ms. The time-delay standard deviation

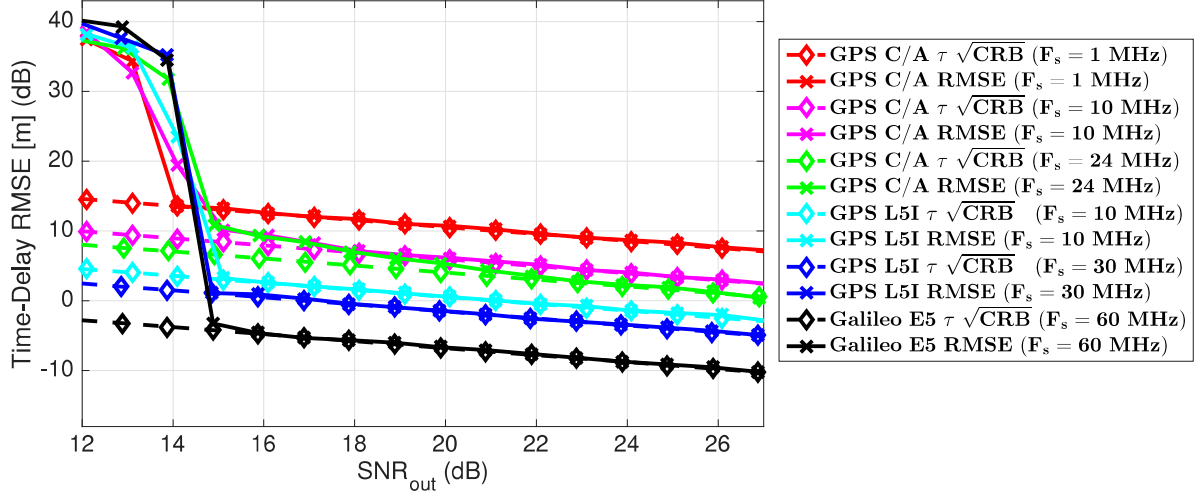


Fig. 4: Time-delay CRB and CMLE: GPS L1 C/A ($F_s = 1, 10, 24$ MHz), GPS L5-I ($F_s = 10, 30$ MHz), and Galileo E5 ($F_s = 60$ MHz).

is: $\sigma_{\tau,L1} = 6.8$ m for $F_s = 1$ MHz, $\sigma_{\tau,L1} = 2.3$ m for $F_s = 10$ MHz and $\sigma_{\tau,L1} = 1.5$ m for $F_s = 24$ MHz, which justifies the interest of exploiting the full signal bandwidth. The drawback is that the CMLE convergence to the CRB is slower w.r.t. the $F_s = 1$ MHz case (i.e., $15 \leq \text{SNR}_{\text{out}} \leq 18$ for $F_s = 10$ MHz and $15 \leq \text{SNR}_{\text{out}} \leq 22$ for $F_s = 24$ MHz), but in any case still having a lower standard deviation w.r.t. lower bandwidths. Second, we can compare these results with larger bandwidth GPS L5 and Galileo E5 signals. Taking as a reference the same receiver operation point $\text{SNR}_{\text{out}} = 25$ dB (F_s in MHz), we obtain the following standard deviations:

- Reference: $\sigma_{\tau,L1} = 1.5$ m ($F_s = 24$ MHz),
- $\sigma_{\tau,L5} = 64$ cm ($F_s = 10$ MHz),
- $\sigma_{\tau,L5} = 39$ cm ($F_s = 30$ MHz),
- $\sigma_{\tau,E5} = 13$ cm ($F_s = 60$ MHz).

These results clearly show the huge time-delay estimation performance improvement that one can achieve using signals with a large bandwidth, and particularly with AltBOC-type signals. For instance, considering the Galileo E5 signal we gain a factor 11 and 3 in time-delay standard deviation w.r.t. to the full bandwidth GPS L1 C/A and L5 signals, respectively.

7.2.2 Phase Estimation:

Notice that the phase CRB in [m] is obtained as $\lambda_c/2\pi\sqrt{\text{CRB}_\varphi}$. We consider first the same value $\lambda_c = \lambda_{L1} = 19.03$ cm for all signals, to understand the asymptotic behavior of the different phase CMLEs. The phase standard deviation for $C/N_0 = 45$ dB-Hz and different $\text{SNR}_{\text{out}} = \{15, 18, 21, 25, 28\}$ dB are $\sigma_\varphi = \{3.8, 2.7, 1.9, 1.2, 0.85\}$ mm, which match the RTK literature where the standard deviation of phase observables is typically in the range of [1–5] mm [58, 59]. It is remarkable that the phase estimation CRB reads $\text{CRB}_\varphi \simeq \frac{1}{2\text{SNR}_{\text{out}}}$ (i.e., equality for real signals), which implies that it does not depend on the broadcast signal but on λ_c and the receiver operation point SNR_{out} , as opposite to the delay estimation. Therefore using fast codes does not improve the phase estimation w.r.t. the legacy GPS L1 C/A signal. In addition, from (4b) we have that the phase CMLE is given by the argument of the cross-ambiguity function evaluated at the delay and Doppler CMLEs. Then, we can expect that if the latter converged to the CRB (i.e., $\text{SNR}_{\text{out}} >$ threshold, around 15 dB, see Section 7.2.1) the same applies to the phase estimate, which is confirmed by the CMLE results in Figure 5. Regardless of λ_c , all signals share the same asymptotic behavior for the phase estimation, which is known to drive the asymptotic RTK performance.

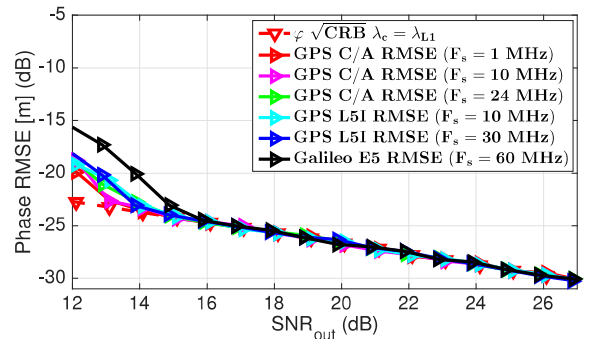


Fig. 5: Phase CRB and CMLE with $\lambda_c = \lambda_{L1}$: GPS L1 C/A ($F_s = 1, 10, 24$ MHz), GPS L5-I ($F_s = 10, 30$ MHz), and Galileo E5 ($F_s = 60$ MHz).

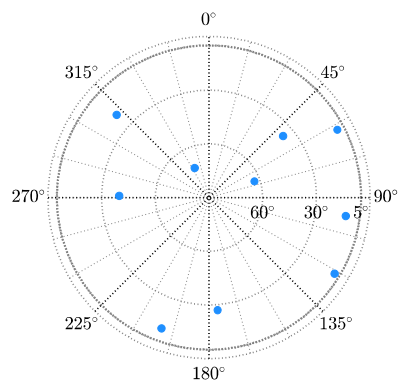


Fig. 6: Skyplot for the experimentation.

7.3 SPP and RTK Scenario Description

The performance characterization of SPP and RTK is based on snapshot of simulated GNSS measurements collected at San Fernando (target receiver) and San Roque (base station for RTK) IGS stations on UTC time 04/03/2020 10:00:00. Considering an elevation mask of five degrees, the resulting constellation was as depicted in Fig. 6. To segregate the role of geometry and satellite availability across GPS and Galileo from the performance of the studied signals, this work considers the satellites from Fig. 6 as generic, common to GPS and Galileo. Next, the SPP and RTK positioning techniques

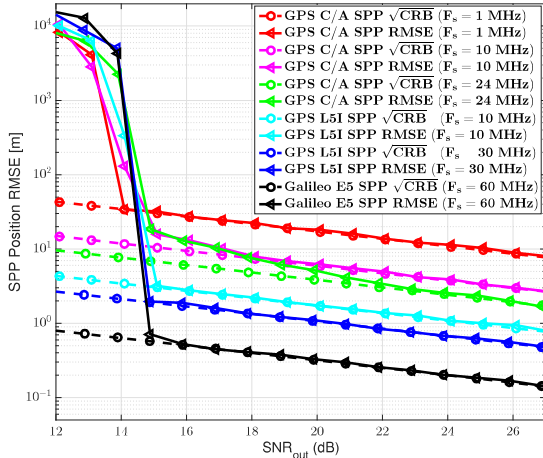


Fig. 7: SPP position CRB (dashed lines) and associated RMSE (solid lines) versus SNR for GPS L1 C/A ($F_s = 1, 10, 24$ MHz), GPS L5-I ($F_s = 10, 30$ MHz), and Galileo E5 ($F_s = 60$ MHz).

will be characterized from a twofold perspective: the estimation of tight lower CRBs and the associated RMSE for the ML estimates for both SPP and RTK positioning methods. The resulting RMSE obtained in the following experiments are, for every signal tested, product of 10^4 Monte Carlo runs.

7.4 Case I: SPP Performance Analysis

Before analyzing the GNSS RTK positioning and clearly see which is the ultimate positioning gain with respect to standard GNSS SPP PVT solutions, we analyze the latter considering the problem formulation in Section 3.3. For this purpose we resort to the CRB derived from (18) with the appropriate matrices \mathbf{D} and \mathbf{C}_n , that is, only considering pseudoranges and not phase observables. Notice that ionospheric, tropospheric and instrumental delays are disregarded in the analysis, since it is of our interest to examine the influence of the different signals, integration times and the receiver operation points rather than the model mismatch of the different atmospheric models typically applied. The CRB and CMLE results for the SPP position computation, considering the different signals in Table 1, are shown in Fig. 7. Again, considering a receiver operation point $\text{SNR}_{\text{out}} = 25$ dB, we obtain the following positioning RMSE:

- GPS L1 C/A $F_s = 1$ MHz - RMSE = 10.3 m.
- GPS L1 C/A $F_s = 10$ MHz - RMSE = 3.3 m.
- GPS L1 C/A $F_s = 24$ MHz - RMSE = 2.36 m.
- GPS L5 $F_s = 10$ MHz - RMSE = 1 m.
- GPS L5 $F_s = 30$ MHz - RMSE = 62.5 cm.
- Galileo E5 $F_s = 60$ MHz - RMSE = 18.5 cm.

For code-based PVT solutions, analogously to the time-delay estimation case in Section 7.2.1, it is clear that using large bandwidth signals such as GPS L5 or Galileo E5 has a huge impact on the achievable positioning precision.

7.5 Case II: RTK Performance Analysis with $\lambda_c = \lambda_{L1}$

As done for the previous SPP case, we want to assess the ultimate achievable performance of RTK positioning techniques and the impact that different GNSS signals may have in such performance. Although it is a common practice for RTK positioning to use multi-constellation/multi-frequency combinations, we are interested in observing the performance gain from every individual GNSS signal. In practice, the characteristics on base and rover receivers may differ, presenting different operation points and/or integration times. For the experimental case at hand, the two receivers are assumed to present the same SNR_{out} and, therefore, the general stochastic model

in (9d) holds valid. First notice that the RTK float solution (i.e., related to the corresponding CRB_{real}) refers to the real estimation part in (11a), that is, disregarding the integer nature of ambiguities. The RTK estimation process follows the three-step decomposition described in (11), where the ILS is resolved based on the LAMBDA method with shrinking search [60]. The RTK fixed solution (i.e., related to the corresponding $\text{CRB}_{\text{real/integer}}$) refers to the estimate of the mixed real-integer LS in (11c), regardless of whether the ILS correctly computes the correct ambiguities. The position RMSE results are summarized in Fig. 8. We can draw the following conclusions:

- i) Notice that the $\text{RTK}_{\text{fixed}}$ solution using the GPS L1 C/A signal with $F_s = 1$ MHz is the same as the $\text{RTK}_{\text{float}}$ solution, that is, the ILS does not correctly fix the ambiguities and therefore the solution obtained is exploring all the ambiguities around the maximum of the code ACF. Notice that higher SNR_{out} values for the GPS L1 C/A signal could be considered, which would involve extending the integration time either coherently or non-coherently. The current configuration with an integration of $T_{\text{bit}} = 20$ ms, which is the coherent integration limit, is not useful for RTK positioning.
- ii) From the previous point, it is clear that if RTK has to be implemented using GPS L1 C/A signals, a higher bandwidth must be considered. For instance, the convergence of the $\text{RTK}_{\text{fixed}}$ to the corresponding $\text{CRB}_{\text{real/integer}}$, using a GPS L1 C/A signal with $F_s = 10$ MHz, is given by $\text{SNR}_{\text{out}} = 26$ dB, which for the maximum coherent integration time $T_I = 20$ ms corresponds to a $C/N_0 = 43$ dB-Hz, which is a nominal value in clear sky conditions. Therefore, a bandwidth around 10 MHz can be taken as a minimum for GPS L1 C/A-based RTK positioning under nominal propagation conditions (i.e., this value matches standard GNSS receiver architectures which typically operate in $F_s \in [8 - 12]$ MHz).
- iii) For any GNSS signal, there exists a threshold receiver operation point for which the $\text{RTK}_{\text{fixed}}$ rapidly converges to the $\text{RTK}_{\text{float}}$ solution. Indeed, once a certain noise level threshold is exceeded (i.e., a delay/phase estimation precision), the use of ILS to fix the ambiguities is not needed. Remarkably, this threshold does not depend on the phase estimation precision but on the code-based delay estimation precision. This is clear in Fig. 8 where we can see that using the Galileo E5 signal we gain $\{10, 7, 3, 2\}$ dB on the SNR_{out} receiver operation threshold point w.r.t. the GPS L1 C/A $F_s = 10$ MHz, GPS L1 C/A $F_s = 24$ MHz, GPS L5-I $F_s = 10$ MHz and GPS L5-I $F_s = 30$ MHz, respectively. Therefore, this clearly justifies the use of fast codes (i.e., both E5 and L5 signals) to provide an improved operation range of RTK architectures.
- iv) The $\text{SNR}_{\text{out}} = 16$ dB RTK threshold for the Galileo E5 signal suggests the validity of this RTK solution in a wide range of applications, i.e., in near-indoor weak signal environments.
- v) To summarize, if a new GNSS signal was designed for precise positioning, the recommendation is to use a carrier frequency as high as possible and a signal modulation with the largest signal bandwidth, the former driving the asymptotic RTK performance and the latter the threshold region.

To complete the discussion, we show that considering the corresponding λ_c for the different signals does not change the asymptotic behavior, therefore these conclusions are valid irrespective of the considered signal.

7.6 Case III: RTK Performance with $\lambda_{L1}, \lambda_{L5}$ and λ_{E5}

7.6.1 Phase Estimation:

In practice we have different wavelengths for each signal: $\lambda_{L1} = 19.03$ cm, $\lambda_{L5} = 25.48$ cm and $\lambda_{E5} = 25.15$ cm. In this case, the phase standard deviations are summarized in Table 2, and the corresponding phase RMSE is given in Fig. 9. The slightly different carrier wavelength induce a slight performance loss using lower frequencies, w.r.t. GPS C/A L1 which uses the higher frequency. This will in turn have an impact on the final RTK performance.

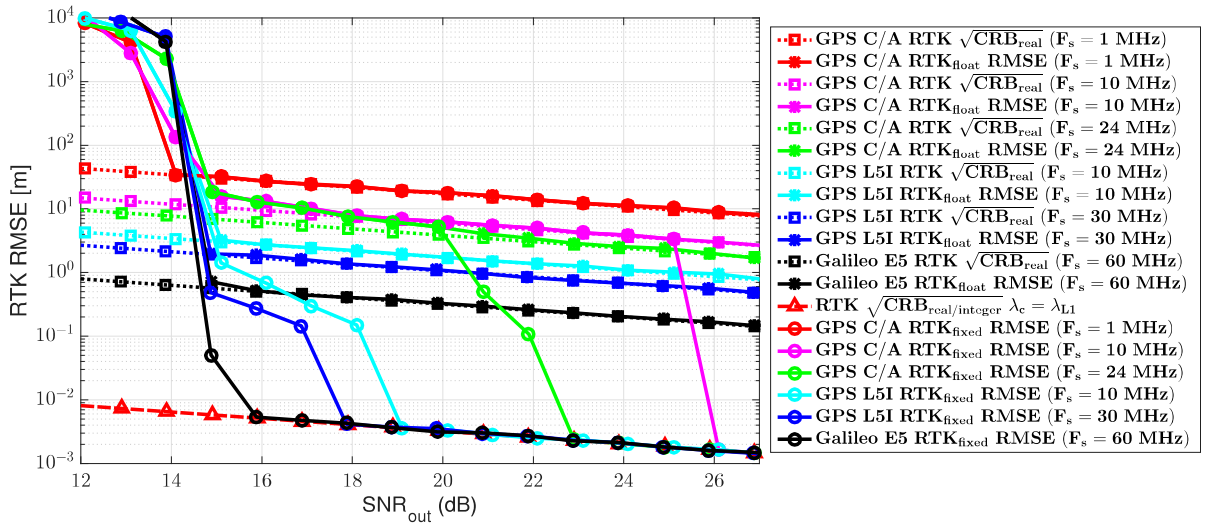


Fig. 8: RTK position CRBs and RMSE with the same $\lambda_c = \lambda_{L1}$, for GPS L1 C/A ($F_s = 1, 10, 24$ MHz), GPS L5-I ($F_s = 10, 30$ MHz), and Galileo E5 ($F_s = 60$ MHz)

Table 2 Phase Estimation Standard Deviation [mm] for different λ_c .

SNR _{out} [dB]	T_I [ms]	$\lambda_{L1}, \sigma_\varphi$ [mm]	$\lambda_{L5}, \sigma_\varphi$ [mm]	$\lambda_{E5}, \sigma_\varphi$ [mm]
15	1	3.8	5.1	5.0
18	2	2.7	3.6	3.6
21	4	1.9	2.6	2.5
25	10	1.2	1.6	1.6
28	20	0.85	1.1	1.1

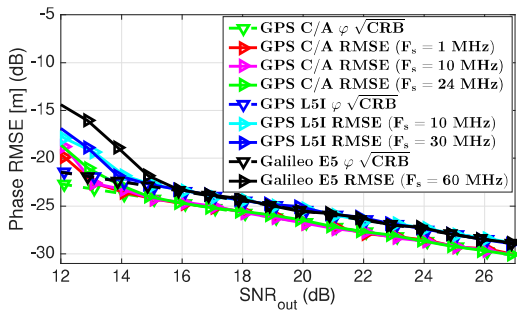


Fig. 9: Phase CRB and CMLE with the corresponding λ_{L1} , λ_{L5} and λ_{E5} : GPS L1 C/A ($F_s = 1, 10, 24$ MHz), GPS L5-I ($F_s = 10, 30$ MHz), and Galileo E5 ($F_s = 60$ MHz).

7.6.2 RTK Performance:

As expected, a slight difference in the phase estimation performance, has a slight impact on the RTK solution, but what is remarkable is that this does not change the asymptotic estimation behavior. The results for different λ_c are summarized in Fig. 10. Notice that we preserve the same SNR threshold regions as in Fig. 8, and the same convergence to the RTK_{float} solutions, therefore the previous conclusions are valid whatever the signal carrier frequency.

8 Conclusions

The main goal of this contribution was to characterize the SPP and RTK estimation performance from the baseband signals. That is, from time-delay and phase estimation, to the final position estimate. Indeed, the input to the standard ML-type positioning solution is the variance of the so-called pseudorange and phase observables which

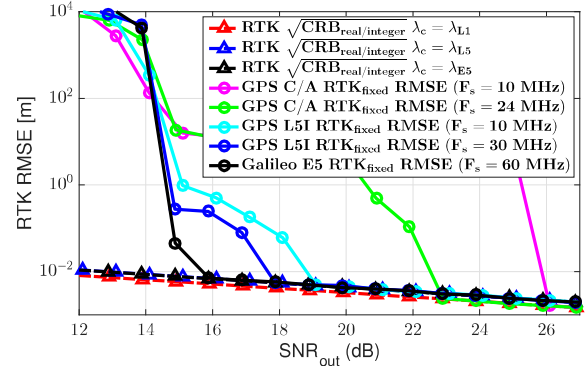


Fig. 10: Figure with different λ_{L1} , λ_{L5} and λ_{E5} .

is in turn determined by the corresponding time-delay and phase estimation precision. In that perspective, a new compact CRB was derived for the joint time-delay, Doppler, phase and amplitude estimation for the narrowband signal model. This CRB is a particular case of a new compact CRB for the generic CSM also provided in this article. A particularly interesting feature is that this new CRB was expressed in terms of the signal samples, making it especially easy to use irrespective of the considered baseband signal. In addition, joint time-delay, Doppler, phase and amplitude estimation using narrowband signals is encountered in a multitude of applications, therefore this tractable CRB constitutes a key tool of broad interest.

Considering the legacy GPS L1 C/A signal as a benchmark and fast codes such as GPS L5 and Galileo E5 signals, it was shown the impact that the GNSS signal has in the different receiver operation steps, and the achievable estimation performance for: i) time-delay estimation, ii) phase estimation, iii) SPP position estimation, and iv) RTK position estimation. A fundamental point with any maximum likelihood estimation procedure is the determination of the threshold region, that is, the SNR value at the output of the matched filter for which the estimator completely deviates from the CRB. It was found that irrespective of the signal considered, the SNR threshold for both time-delay and phase estimation is around 15 dB. This was also the case for the SPP code-based position estimation, for which it was shown that using a Galileo E5 signal can provide a huge performance gain, potentially reaching standard deviations below 20 cm.

For RTK positioning, the new CRB and the proposed analysis provided even more interesting results. In fact, it was shown that the SNR threshold region is driven by the time-delay precision and not

the phase one. Using fast codes we may have up to 10 dB of gain in the threshold, which in turn implies the validity of such RTK solutions in a wider range of applications. Also, notice that this threshold can be used to determine for which operation regions it is worth to exploit phase measurements, because above the threshold the RTK fixed solution rapidly converges to the float (i.e., real) one. These results hold whatever the signal carrier frequency. To summarize, if a new GNSS signal was to be designed for precise positioning, the recommendation would be to use a carrier frequency as high as possible and a signal modulation with the largest signal bandwidth, the former driving the asymptotic RTK performance, and the latter the threshold region.

Acknowledgments

This research was partially supported by the DGA/AID projects (2019.65.0068.00.470.75.01, 2018.60.0072.00.470.75.01), the TéSA Lab Postdoctoral Research Fellowship, and the National Science Foundation under Awards CNS-1815349 and ECCS-1845833.

9 References

- 1 Trees, H.L.V.: ‘Detection, estimation, and modulation theory, Part III: Radar – Sonar Signal Processing and Gaussian Signals in Noise’. (John Wiley & Sons, 2001)
- 2 Chen, J., Huang, Y., Benesty, J. ‘Time delay estimation’. In: Huang, Y., Benesty, J., editors. *Audio Signal Processing for Next-Generation Multimedia Communication Systems*. (Boston, MA, USA: Springer, 2004. pp. 197–227)
- 3 Levy, B.C.: ‘Principles of Signal Detection and Parameter Estimation’. (Springer, 2008)
- 4 Mengali, U., D’Andrea, A.N.: ‘Synchronization Techniques for Digital Receivers’. (New York, USA: Plenum Press, 1997)
- 5 Fernández.Prades, C., Lo Presti, L., Falletti, E.: ‘Satellite radiolocation from GPS to GNSS and beyond: novel technologies and applications for civil mass market’, *Proc of the IEEE*, 2011, **99**, (11), pp. 1882–1904
- 6 Amin, M.G., Closas, P., Broumandan, A., Volakis, J.L.: ‘Vulnerabilities, threats, and authentication in satellite-based navigation systems [scanning the issue]’, *Proceedings of the IEEE*, 2016, **104**, (6), pp. 1169–1173
- 7 Yan, J., et al.: ‘Review of range-based positioning algorithms’, *IEEE Trans Aerosp Electron Syst*, 2013, **28**, (8), pp. 2–27
- 8 Zavorotny, V.U., Gleason, S., Cardellach, E., Camps, A.: ‘Tutorial on remote sensing using GNSS bistatic radar of opportunity’, *IEEE Geosci Remote Sens Mag*, 2014, **2**, (4), pp. 8–45
- 9 Lestarcuit, L., et al.: ‘Reflectometry With an Open-Source Software GNSS Receiver: Use Case With Carrier Phase Altimetry’, *IEEE Journal of Selected Topics in Applied Earth Observations and Remote Sensing*, 2016, **9**, (10), pp. 4843–4853
- 10 Cardellach, E., et al.: ‘First Precise Spaceborne Sea Surface Altimetry With GNSS Reflected Signals’, *IEEE J Select Topics Appl Earth Observ Remote Sensing*, 2019, **13**, pp. 102–112
- 11 Schreier, P.J., Scharf, L.L.: ‘Statistical Signal Processing of Complex-Valued Data’. (Cambridge University Press, 2010)
- 12 Schewpke, F.C.: ‘Sensor array data processing for multiple signal sources’, *IEEE Trans Information Theory*, 1968, **14**, pp. 294–305
- 13 Stoica, P., Nehorai, A.: ‘Performances study of conditional and unconditional direction of arrival estimation’, *IEEE Trans Acoust, Speech, Signal Process*, 1990, **38**, (10), pp. 1783–1795
- 14 Scharf, L.L.: ‘Statistical signal processing: detection, estimation, and time series analysis’. (Addison-Wesley, 2002)
- 15 Trees, H.L.V.: ‘Optimum Array Processing’. (Wiley-Interscience, New-York, 2002)
- 16 Renaux, A., Forster, P., Chaumette, E., Larzabal, P.: ‘On the high-SNR conditional maximum-likelihood estimator full statistical characterization’, *IEEE Trans Signal Process*, 2006, **54**, (12), pp. 4840 – 4843
- 17 Ottersten, B., Viberg, M., Stoica, P., Nehorai, A. ‘Exact and large sample maximum likelihood techniques for parameter estimation and detection in array processing’. In: Haykin, S., Litva, J., Shepherd, T.J., editors. *Radar Array Processing*. (Heidelberg: Springer-Verlag, 1993. pp. 99–151)
- 18 Tsao, J., Steinberg, B.D.: ‘Reduction of Sidelobe and Speckle Artifacts in Microwave Imaging: the CLEAN Technique’, *IEEE Trans Antennas and Propagation*, 1988, **36**, (4), pp. 543–556
- 19 Ziskind, I., Wax, M.: ‘Maximum likelihood localization of multiple sources by alternating projection’, *IEEE Trans Acoustics, Speech, and Signal Processing*, 1988, **36**, (10), pp. 1553–1560
- 20 Stoica, P., Söderström, T.: ‘On reparametrization of loss functions used in estimation and the invariance principle’, *Signal Processing*, 1989, **17**, pp. 383–387
- 21 Antreich, F., Nossek, J.A., Seco.Granados, G., Swindlehurst, A.L.: ‘The extended invariance principle for signal parameter estimation in an unknown spatial field’, *IEEE Trans Signal Process*, 2011, **59**, (7), pp. 3213–3225
- 22 Swindlehurst, A.L., Stoica, P.: ‘Maximum likelihood methods in radar array signal processing’, *Proc IEEE*, 1998, **86**, (2), pp. 421–441
- 23 Vincent, F., Chaumette, E., Charbonnier, C., Israel, J., J Ries, L., Aubourg, M., et al.: ‘Asymptotically Efficient GNSS Trilateration’, *Signal Processing*, 2017, **133**, pp. 270–277
- 24 Closas, P., Fernández.Prades, C., Fernández.Rubio, J.A.: ‘Maximum likelihood estimation of position in gnss’, *IEEE Signal Processing letters*, 2007, **14**, (5), pp. 359–362
- 25 Closas, P., Gusi.Amigó, A.: ‘Direct position estimation of GNSS receivers: Analyzing main results, architectures, enhancements, and challenges’, *IEEE Signal Processing Magazine*, 2017, **34**, (5), pp. 72–84
- 26 Eueler, H.J., Goad, C.C.: ‘On optimal filtering of gps dual frequency observations without using orbit information’, *Bulletin géodésique*, 1991, **65**, (2), pp. 130–143
- 27 Kuusniemi, H., Wieser, A., Lachapelle, G., Takala, J.: ‘User-level reliability monitoring in urban personal satellite-navigation’, *IEEE Transactions on Aerospace and Electronic Systems*, 2007, **43**, (4), pp. 1305–1318
- 28 Medina, D., Gibson, K., Ziebold, R., Closas, P.: ‘Determination of pseudorange error models and multipath characterization under signal-degraded scenarios’. In: *Proceedings of the 31st International Technical Meeting of the Satellite Division of The Institute of Navigation (ION GNSS+ 2018)*. (, 2018. pp. 24–28)
- 29 Dogandžić, A., Nehorai, A.: ‘Cramér-Rao bounds for estimating range, velocity, and direction with an active array’, *IEEE Trans Signal Process*, 2001, **49**, (6), pp. 1122–1137
- 30 Noels, N., Wymersch, H., Steendam, H., Moeneclaey, M.: ‘True Cramér-Rao bound for timing recovery from a bandlimited linearly modulated waveform with unknown carrier phase and frequency’, *IEEE Trans on Communications*, 2004, **52**, (3), pp. 473–483
- 31 Closas, P., Fernández.Prades, C., Fernández.Rubio, J.A.: ‘Cramér-Rao bound analysis of positioning approaches in GNSS receivers’, *IEEE Trans on Signal Processing*, 2009, **57**, (10), pp. 3775–3786
- 32 Enneking, C., et al.: ‘Multi-satellite time-delay estimation for reliable high-resolution GNSS receivers’. In: *Proc. of the IEEE/ION PLANS*. (Myrtle Beach, SC, USA, 2012).
- 33 Chen, Y., Blum, R.S.: ‘On the Impact of Unknown Signals on Delay, Doppler, Amplitude, and Phase Parameter Estimation’, *IEEE Trans Signal Process*, 2019, **67**, (2), pp. 431–443
- 34 Bartov, A., Messer, H.: ‘Lower bound on the achievable DSP performance for localizing step-like continuous signals in noise’, *IEEE Trans Signal Process*, 1998, **46**, (8), pp. 2195–2201
- 35 Kay, S.M.: ‘Fundamentals of Statistical Signal Processing: Estimation Theory’. (Englewood Cliffs, New Jersey, USA: Prentice-Hall, 1993)
- 36 Yau, S.F., Bresler, Y.: ‘A compact Cramér-Rao bound expression for parametric estimation of superimposed signals’, *IEEE Trans Signal Process*, 1992, **40**, (5), pp. 1226–1230
- 37 Williams, N., Wu, G., Closas, P.: ‘Impact of positioning uncertainty on eco-approach and departure of connected and automated vehicles’. In: *2018 IEEE/ION Position, Location and Navigation Symposium (PLANS)*. (IEEE, 2018. pp. 1081–1087)
- 38 Teunissen, P.J.G., Montenbruck, O., editors. ‘Handbook of Global Navigation Satellite Systems’. (Switzerland: Springer, 2017)
- 39 Rife, D.C., Boorstyn, R.R.: ‘Single tone parameter estimation from discrete-time observations’, *IEEE Trans Information Theory*, 1974, **20**, (5), pp. 591–598
- 40 D’Andrea, A.N., Mengali, U., Reggiannini, R.: ‘The modified Cramér-Rao bound and its application to synchronization problems’, *IEEE Trans Communications*, 1994, **42**, (2/3/4), pp. 1391–1399
- 41 Smith, S.T.: ‘Statistical resolution limits and the complexified Cramér Rao bound’, *IEEE Trans Signal Process*, 2005, **53**, (5), pp. 1597–1609
- 42 El Korso, M.N., Boyer, R., Renaux, A., Marcos, S.: ‘Conditional and Unconditional Cramér-Rao Bounds for Near-Field Source Localization’, *IEEE Trans Signal Process*, 2010, **58**, (5), pp. 2901–2907
- 43 Wu, N., Wang, H., Zhao, H., Liu, H., Kuang, J.: ‘Evaluation of cramér-rao bounds for phase estimation of coded linearly modulated signals’. (Proc. IEEE Vehicular Technology Conference, 2014).
- 44 Steendam, H., Moeneclaey, M.: ‘Low-SNR limit of the Cramér-Rao bound for estimating the time-delay of a PSK, QAM, or PAM waveform’, *IEEE Commun Letters*, 2001, **5**, (1), pp. 31–33
- 45 Trees, H.L.V., Bell, K.L., Tian, Z.: ‘Detection, Estimation and Modulation Theory - Part I’. 2nd ed. (Wiley, 2013)
- 46 Wang, P., Orlitzki, P.V., Sadamoto, K., Tsujita, W., Sawa, Y.: ‘Cramér–Rao Bounds for a Coupled Mixture of Polynomial Phase and Sinusoidal FM Signals’, *IEEE Signal Process Letters*, 2017, **24**, (6), pp. 746–750
- 47 Das, P., Vilà-Valls, J., Chaumette, E., Vincent, F., Davain, L., Bonnabel, S.: ‘On the accuracy limit of time-delay estimation with a band-limited signal’. In: *Proc. of the IEEE Intl. Conf. on Acoustics, Speech and Signal Processing (ICASSP)*. (Brighton, UK, 2019).
- 48 Medina, D., Vilà-Valls, J., Chaumette, E., Vincent, F., Closas, P.: ‘Cramér–Rao bound for a mixture of real- and integer-valued parameter vectors and its application to the linear regression model’, *Submitted to Signal Processing - under 1st round of reviews*, 2020,
- 49 Betz, J.W.: ‘Binary offset carrier modulations for radionavigation’, *Navigation*, 2001, **48**, (4), pp. 227–246
- 50 Teunissen, P.J.G.: ‘Least-squares estimation of the integer GPS ambiguities’. In: *Invited lecture, Section IV Theory and Methodology*. IAG General Meeting. (Beijing, China, 1993).
- 51 Teunissen, P.J.: ‘An optimality property of the integer least-squares estimator’, *Journal of geodesy*, 1999, **73**, (11), pp. 587–593
- 52 Teunissen, P.: ‘Integer aperture GNSS ambiguity resolution’, *Artificial Satellites*, 2003, **38**, (3), pp. 79–88
- 53 Teunissen, P.J.G.: ‘The LAMBDA Method for the GNSS Compass’, *Artificial Satellites*, 2006, **41**, (3), pp. 89–103

- 54 Teunissen, P.: 'The probability distribution of the gps baseline for a class of integer ambiguity estimators'. *Journal of Geodesy*, 1999, **73**, (5), pp. 275–284
 55 Rodriguez, J.Á.Á.: 'On Generalized Signal Waveforms for Satellite Navigation'. (Universitätsbibliothek der Universität der Bundeswehr München, 2008). Available from: <https://books.google.fr/books?id=dd3wsAAACAAJ>
 56 'Interface Specification IS-GPS-705D NavStar GPS Space Segment / UserSegment L5 Interface'. (, 2014.
 57 Lestarquit, L., Artaud, G., Issler, J.L. 'Altboc for dummies or everything you always wanted to know about altboc'. In: ION GNSS. (, 2008. pp. 961–970
 58 Odolinski, R., Teunissen, P., Odijk, D.: 'Combined gps+ bds for short to long baseline rtk positioning', *Measurement Science and Technology*, 2015, **26**, (4), pp. 045801
 59 Odolinski, R., Teunissen, P.J.: 'Single-frequency, dual-GNSS versus dual-frequency, single-GNSS: a low-cost and high-grade receivers GPS-BDS RTK analysis', *Journal of geodesy*, 2016, **90**, (11), pp. 1255–1278
 60 DeJonge, P., Tiberius, C., et al.: 'The LAMBDA Methods for Integer Ambiguity Estimation: Implementation Aspects'. vol. 12. (Verlag der Delft Univers. of Technolog., 1996)
 61 Seber, G.A.F.: 'Matrix Handbook for Statisticians'. (Wiley Series in Probability and Statistics, 2008)

10 Proof of the Compact CRB Expression for the Single Source CSM in Section 4

In the following: i) $\underline{\mathbf{y}} = \begin{bmatrix} \operatorname{Re}\{\mathbf{y}\} \\ \operatorname{Im}\{\mathbf{y}\} \end{bmatrix}$, $\forall \mathbf{y} \in \mathbb{C}^{N_1 \times N_2}$, and ii) for the sake of simplicity we denote $\underline{\mathbf{a}}' \triangleq \underline{\mathbf{a}}'(\boldsymbol{\theta})$, $\mathbf{a} \triangleq \mathbf{a}(\boldsymbol{\eta})$. Then (13) can be recast as

$$\underline{\mathbf{x}} = \underline{\mathbf{a}}'(\boldsymbol{\theta})\rho + \underline{\mathbf{n}}, \quad \underline{\mathbf{n}} \sim \mathcal{N}(\mathbf{0}, \sigma_n^2 \mathbf{I}_{2N}/2), \quad \boldsymbol{\epsilon}^\top = (\sigma_n^2, \rho, \boldsymbol{\theta}^\top). \quad (21)$$

Since $\underline{\mathbf{x}} \sim \mathcal{N}(\mathbf{m}_{\underline{\mathbf{x}}}(\boldsymbol{\epsilon}), \mathbf{C}_{\underline{\mathbf{x}}}(\boldsymbol{\epsilon}))$, the Fisher information matrix (FIM) is given by the Slepian-Bangs formula [15]

$$(\mathbf{F}_\boldsymbol{\epsilon})_{k,l} = \frac{\partial \mathbf{m}_{\underline{\mathbf{x}}}(\boldsymbol{\epsilon})}{\partial \epsilon_k}^\top \mathbf{C}_{\underline{\mathbf{x}}}^{-1}(\boldsymbol{\epsilon}) \frac{\partial \mathbf{m}_{\underline{\mathbf{x}}}(\boldsymbol{\epsilon})}{\partial \epsilon_l} + \frac{1}{2} \operatorname{tr} \left(\mathbf{C}_{\underline{\mathbf{x}}}^{-1}(\boldsymbol{\epsilon}) \frac{\partial \mathbf{C}_{\underline{\mathbf{x}}}(\boldsymbol{\epsilon})}{\partial \epsilon_k} \mathbf{C}_{\underline{\mathbf{x}}}^{-1}(\boldsymbol{\epsilon}) \frac{\partial \mathbf{C}_{\underline{\mathbf{x}}}(\boldsymbol{\epsilon})}{\partial \epsilon_l} \right).$$

In (21), as $\mathbf{m}_{\underline{\mathbf{x}}}(\boldsymbol{\epsilon}) = \underline{\mathbf{a}}'(\boldsymbol{\theta})\rho$ and $\mathbf{C}_{\underline{\mathbf{x}}}(\boldsymbol{\epsilon}) = \sigma_n^2/2\mathbf{I}_{2N}$, then

$$\begin{aligned} \text{CRB}_\boldsymbol{\epsilon} &= \mathbf{F}_\boldsymbol{\epsilon}^{-1} = \begin{bmatrix} \frac{\sigma_n^4}{N} & \mathbf{0}^\top \\ \mathbf{0} & \text{CRB}_{(\rho, \boldsymbol{\theta})} \end{bmatrix}, \\ \text{CRB}_{(\rho, \boldsymbol{\theta})} &= \frac{\sigma_n^2}{2} \begin{bmatrix} \|\underline{\mathbf{a}}'\|_\top^2 & \rho \underline{\mathbf{a}}'^\top \frac{\partial \underline{\mathbf{a}}'}{\partial \boldsymbol{\theta}^\top} \\ \rho \frac{\partial \underline{\mathbf{a}}'}{\partial \boldsymbol{\theta}^\top} \underline{\mathbf{a}}' & \rho^2 \frac{\partial \underline{\mathbf{a}}'}{\partial \boldsymbol{\theta}^\top} \frac{\partial \underline{\mathbf{a}}'}{\partial \boldsymbol{\theta}^\top} \end{bmatrix}^{-1}. \end{aligned}$$

By resorting to the block matrix inversion lemma [61, p 309],

$$\begin{aligned} \begin{bmatrix} \mathbf{A}_{11} & \mathbf{A}_{12} \\ \mathbf{A}_{21} & \mathbf{A}_{22} \end{bmatrix}^{-1} &= \begin{bmatrix} \mathbf{C}_1^{-1} & -\mathbf{A}_{11}^{-1} \mathbf{A}_{12} \mathbf{C}_2^{-1} \\ -\mathbf{C}_2^{-1} \mathbf{A}_{21} \mathbf{A}_{11}^{-1} & \mathbf{C}_2^{-1} \end{bmatrix}, \\ \mathbf{C}_1 &= \mathbf{A}_{11} - \mathbf{A}_{12} \mathbf{A}_{22}^{-1} \mathbf{A}_{21}, \quad \mathbf{C}_2 = \mathbf{A}_{22} - \mathbf{A}_{21} \mathbf{A}_{11}^{-1} \mathbf{A}_{12}, \\ \mathbf{C}_1^{-1} &= \mathbf{A}_{11}^{-1} + \mathbf{A}_{11}^{-1} \mathbf{A}_{12} \mathbf{C}_2^{-1} \mathbf{A}_{21} \mathbf{A}_{11}^{-1}, \end{aligned}$$

one obtains

$$\begin{aligned} \text{CRB}_\rho &= \frac{\sigma_n^2}{2} \left(\underline{\mathbf{a}}'^\top \mathbf{\Pi}_{\frac{\partial \underline{\mathbf{a}}'}{\partial \boldsymbol{\theta}^\top}}^\perp \underline{\mathbf{a}}' \right)^{-1}, \\ \text{CRB}_\boldsymbol{\theta} &= \frac{\sigma_n^2}{2\rho^2} \Phi_\boldsymbol{\theta}^{-1}, \quad \Phi_\boldsymbol{\theta} = \left(\frac{\partial \underline{\mathbf{a}}'}{\partial \boldsymbol{\theta}^\top} \right)^\top \mathbf{\Pi}_{\underline{\mathbf{a}}'}^\perp \frac{\partial \underline{\mathbf{a}}'}{\partial \boldsymbol{\theta}^\top}. \end{aligned}$$

Moreover, since

$$\begin{aligned} \underline{\mathbf{A}}^\top \underline{\mathbf{B}} &= \operatorname{Re}\{\underline{\mathbf{A}}\}^\top \operatorname{Re}\{\underline{\mathbf{B}}\} + \operatorname{Im}\{\underline{\mathbf{A}}\}^\top \operatorname{Im}\{\underline{\mathbf{B}}\} \\ &= \operatorname{Re}\{\underline{\mathbf{A}}^\top \underline{\mathbf{B}}\} \end{aligned}$$

then

$$\begin{aligned} \underline{\mathbf{a}}'^\top \underline{\mathbf{a}}' &= \mathbf{a}^\top \mathbf{a}, \\ \underline{\mathbf{a}}'^\top \frac{\partial \underline{\mathbf{a}}'}{\partial \boldsymbol{\theta}^\top} &= \left(\begin{array}{cc} 0 & \operatorname{Re}\left\{\mathbf{a}^\top \frac{\partial \mathbf{a}}{\partial \boldsymbol{\eta}^\top}\right\} \end{array} \right) \\ \left(\frac{\partial \underline{\mathbf{a}}'}{\partial \boldsymbol{\theta}^\top} \right)^\top \frac{\partial \underline{\mathbf{a}}'}{\partial \boldsymbol{\theta}^\top} &= \operatorname{Re} \left\{ \begin{bmatrix} \|\mathbf{a}\|^2 & -j \mathbf{a}^\top \frac{\partial \mathbf{a}}{\partial \boldsymbol{\eta}^\top} \\ j \frac{\partial \mathbf{a}}{\partial \boldsymbol{\eta}^\top} \mathbf{a} & \frac{\partial \mathbf{a}}{\partial \boldsymbol{\eta}^\top}^\top \frac{\partial \mathbf{a}}{\partial \boldsymbol{\eta}^\top} \end{bmatrix} \right\} \\ \left(\frac{\partial \underline{\mathbf{a}}'}{\partial \boldsymbol{\theta}^\top} \right)^\top \frac{\partial \underline{\mathbf{a}}'}{\partial \boldsymbol{\theta}^\top} &= \begin{bmatrix} \|\mathbf{a}\|^2 & \operatorname{Im}\left\{\mathbf{a}^\top \frac{\partial \mathbf{a}}{\partial \boldsymbol{\eta}^\top}\right\} \\ \operatorname{Im}\left\{\mathbf{a}^\top \frac{\partial \mathbf{a}}{\partial \boldsymbol{\eta}^\top}\right\}^\top & \operatorname{Re}\left\{\frac{\partial \mathbf{a}}{\partial \boldsymbol{\eta}^\top} \frac{\partial \mathbf{a}}{\partial \boldsymbol{\eta}^\top}\right\} \end{bmatrix} \end{aligned}$$

and therefore

$$\begin{aligned} \Phi_\boldsymbol{\theta} &= \frac{\partial \underline{\mathbf{a}}'}{\partial \boldsymbol{\theta}^\top}^\top \frac{\partial \underline{\mathbf{a}}'}{\partial \boldsymbol{\theta}^\top} - \frac{1}{\underline{\mathbf{a}}'^\top \underline{\mathbf{a}}'} \left(\underline{\mathbf{a}}'^\top \frac{\partial \underline{\mathbf{a}}'}{\partial \boldsymbol{\theta}^\top} \right)^\top \left(\underline{\mathbf{a}}'^\top \frac{\partial \underline{\mathbf{a}}'}{\partial \boldsymbol{\theta}^\top} \right) \\ &= \begin{bmatrix} \|\mathbf{a}\|^2 & \operatorname{Im}\{\boldsymbol{\Upsilon}\}^\top \\ \operatorname{Im}\{\boldsymbol{\Upsilon}\} & \operatorname{Re}\{\boldsymbol{\Upsilon}\} - \frac{\operatorname{Re}\{\boldsymbol{\gamma}\} \operatorname{Re}\{\boldsymbol{\gamma}\}^\top}{\|\mathbf{a}\|^2} \end{bmatrix}, \end{aligned}$$

where $\boldsymbol{\Upsilon} = \frac{\partial \mathbf{a}}{\partial \boldsymbol{\eta}^\top}^\top \frac{\partial \mathbf{a}}{\partial \boldsymbol{\eta}^\top}$ and $\boldsymbol{\gamma}^\top = \mathbf{a}^\top \frac{\partial \mathbf{a}}{\partial \boldsymbol{\eta}^\top}$, which yields

$$\begin{aligned} \Phi_\boldsymbol{\theta}^{-1} &= \begin{bmatrix} \mathbf{C}_1^{-1} & -\frac{\mathbf{A}_{12}}{A_{11}} \mathbf{C}_2^{-1} \\ -\mathbf{C}_2^{-1} \frac{\mathbf{A}_{21}}{A_{11}} & \mathbf{C}_2^{-1} \end{bmatrix}, \\ \mathbf{C}_2 &= \operatorname{Re}\{\boldsymbol{\Upsilon}\} - \frac{\operatorname{Re}\{\boldsymbol{\gamma}\} \operatorname{Re}\{\boldsymbol{\gamma}\}^\top + \operatorname{Im}\{\boldsymbol{\gamma}\} \operatorname{Im}\{\boldsymbol{\gamma}\}^\top}{\|\mathbf{a}\|^2} \\ &= \operatorname{Re}\{\boldsymbol{\Upsilon}\} - \frac{\operatorname{Re}\{\boldsymbol{\gamma} \boldsymbol{\gamma}^H\}}{\|\mathbf{a}\|^2} = \operatorname{Re} \left\{ \frac{\partial \mathbf{a}}{\partial \boldsymbol{\eta}^\top}^\top \mathbf{\Pi}_{\mathbf{a}}^\perp \frac{\partial \mathbf{a}}{\partial \boldsymbol{\eta}^\top} \right\} \\ \mathbf{C}_1^{-1} &= \frac{1}{\|\mathbf{a}\|^2} + \frac{\operatorname{Im}\{\boldsymbol{\gamma}\}^\top \mathbf{C}_2^{-1} \operatorname{Im}\{\boldsymbol{\gamma}\}}{\|\mathbf{a}\|^4} \\ \mathbf{C}_2^{-1} \frac{\mathbf{A}_{21}}{A_{11}} &= \frac{\mathbf{C}_2^{-1} \operatorname{Im}\{\boldsymbol{\gamma}\}}{\|\mathbf{a}\|^2}, \end{aligned}$$

that is, the expressions in (14c)–(14f). Last, to obtain (14a) consider that

$$\begin{aligned} \underline{\mathbf{a}}'^\top \mathbf{\Pi}_{\frac{\partial \underline{\mathbf{a}}'}{\partial \boldsymbol{\theta}^\top}}^\perp \underline{\mathbf{a}}' &= \mathbf{a}^\top \mathbf{a} - \left(\operatorname{Re}\{\boldsymbol{\gamma}\} \right)^\top \\ &\times \begin{bmatrix} \mathbf{a}^\top \mathbf{a} & \operatorname{Im}\{\boldsymbol{\gamma}\}^\top \\ \operatorname{Im}\{\boldsymbol{\gamma}\} & \operatorname{Re}\{\boldsymbol{\Upsilon}\} \end{bmatrix}^{-1} \begin{pmatrix} 0 \\ \operatorname{Re}\{\boldsymbol{\gamma}\} \end{pmatrix} \\ &= \mathbf{a}^\top \mathbf{a} - \operatorname{Re}\{\boldsymbol{\gamma}\}^\top \left(\operatorname{Re}\{\boldsymbol{\Upsilon}\} - \frac{\operatorname{Im}\{\boldsymbol{\gamma}\} \operatorname{Im}\{\boldsymbol{\gamma}\}^\top}{\mathbf{a}^\top \mathbf{a}} \right)^{-1} \operatorname{Re}\{\boldsymbol{\gamma}\} \\ &= \mathbf{a}^\top \mathbf{a} - \operatorname{Re}\{\boldsymbol{\gamma}\}^\top \left(\mathbf{C}_2 + \frac{\operatorname{Re}\{\boldsymbol{\gamma}\} \operatorname{Re}\{\boldsymbol{\gamma}\}^\top}{\mathbf{a}^\top \mathbf{a}} \right)^{-1} \operatorname{Re}\{\boldsymbol{\gamma}\} \\ &= \mathbf{a}^\top \mathbf{a} - \operatorname{Re}\{\boldsymbol{\gamma}\}^\top \frac{\mathbf{a}^\top \mathbf{a} \mathbf{C}_2^{-1} \operatorname{Re}\{\boldsymbol{\gamma}\}}{\mathbf{a}^\top \mathbf{a} + \operatorname{Re}\{\boldsymbol{\gamma}\}^\top \mathbf{C}_2^{-1} \operatorname{Re}\{\boldsymbol{\gamma}\}} \\ \underline{\mathbf{a}}'^\top \mathbf{\Pi}_{\frac{\partial \underline{\mathbf{a}}'}{\partial \boldsymbol{\theta}^\top}}^\perp \underline{\mathbf{a}}' &= \frac{\left(\mathbf{a}^\top \mathbf{a} \right)^2}{\mathbf{a}^\top \mathbf{a} + \operatorname{Re}\{\boldsymbol{\gamma}\}^\top \mathbf{C}_2^{-1} \operatorname{Re}\{\boldsymbol{\gamma}\}}, \end{aligned}$$

$$\text{CRB}_\rho = \frac{\sigma_n^2}{2 \mathbf{a}^\top \mathbf{a}} \left(1 + \frac{\operatorname{Re}\{\boldsymbol{\gamma}\}^\top \mathbf{C}_2^{-1} \operatorname{Re}\{\boldsymbol{\gamma}\}}{\mathbf{a}^\top \mathbf{a}} \right).$$

As an example, we consider the well-known single tone (η) estimation problem [39]:

$$\begin{aligned}\mathbf{a}(\eta) &= (1, e^{j2\pi\eta}, \dots, e^{j2\pi\eta(N-1)})^\top, \|\mathbf{a}(\eta)\|^2 = N, \\ \mathbf{a}(\eta)^H \frac{\partial \mathbf{a}(\eta)}{\partial \eta} &= j2\pi P, \frac{\partial \mathbf{a}(\eta)}{\partial \eta}^H \frac{\partial \mathbf{a}(\eta)}{\partial \eta} = (2\pi)^2 Q, \\ P &= \sum_{n=0}^{N-1} n = \frac{N(N-1)}{2}, \\ Q &= \sum_{n=0}^{N-1} n^2 = \frac{N(N-1)(2N-1)}{6},\end{aligned}$$

which yields

$$\left\{ \begin{array}{l} CRB_\eta = \frac{\sigma_n^2}{2\rho^2} \frac{1}{(2\pi)^2 \left(Q - \frac{P^2}{N}\right)} = \frac{\sigma_n^2}{\rho^2} \frac{6}{N(N^2-1)} \frac{1}{(2\pi)^2} \\ CRB_\varphi = \frac{\sigma_n^2}{2\rho^2} \frac{1}{N - \frac{P^2}{Q}} = \frac{\sigma_n^2}{\rho^2} \frac{2N-1}{N(N+1)} \\ CRB_\rho = \frac{\sigma_n^2}{2N} \end{array} \right. \quad (22a)$$

11 Proof of the CRB Expression for the Narrowband Signal Model in Section 5

First notice that

$$\begin{aligned}\text{CRB}_\eta &= \frac{\sigma_n^2}{2\rho^2} \Phi_\eta^{-1} \\ \Phi_\eta &= \lim_{(N'_1, N'_2) \rightarrow (-\infty, +\infty)} \text{Re} \left\{ \left(\frac{\partial \mathbf{a}(\eta)}{\partial \eta^\top} \right)^H \boldsymbol{\Pi}_{\mathbf{a}(\eta)}^\perp \frac{\partial \mathbf{a}(\eta)}{\partial \eta^\top} \right\}.\end{aligned}$$

The derivative of $a(t; \eta)$ w.r.t. the parameters of interest reads

$$\begin{aligned}\frac{\partial a(t; \eta)}{\partial \eta} &= -\mathbf{Q} \boldsymbol{\vartheta}(t - \tau) e^{-j\omega_c b(t - \tau)}, \\ \mathbf{Q} &= \begin{bmatrix} -j\omega_c b & 0 & 1 \\ 0 & j\omega_c & 0 \end{bmatrix}, \boldsymbol{\vartheta}(t) = \begin{pmatrix} c(t) \\ tc(t) \\ c^{(1)}(t) \end{pmatrix}.\end{aligned}$$

where $c^{(1)}(t) = \frac{dc(t)}{dt}$. Then we can write

$$\begin{aligned}\mathbf{a}^H(\eta) \frac{\partial \mathbf{a}(\eta)}{\partial \eta^\top} &= - \left(\mathbf{Q} \sum_{n=N'_1}^{N'_2} \boldsymbol{\vartheta}(nT_s - \tau) c(nT_s - \tau)^* \right)^\top, \\ \frac{\partial \mathbf{a}(\eta)}{\partial \eta^\top}^H \frac{\partial \mathbf{a}(\eta)}{\partial \eta^\top} &= \mathbf{Q}^* \left(\sum_{n=N'_1}^{N'_2} \boldsymbol{\vartheta}(nT_s - \tau) \boldsymbol{\vartheta}^H(nT_s - \tau) \right) \mathbf{Q}^\top \\ \|\mathbf{a}(\eta)\|^2 &= \sum_{n=N'_1}^{N'_2} |c(nT_s - \tau)|^2,\end{aligned}$$

and

$$\begin{aligned}\lim_{(N'_1, N'_2) \rightarrow (-\infty, +\infty)} T_s \sum_{n=N'_1}^{N'_2} \boldsymbol{\vartheta}(nT_s - \tau) c(nT_s - \tau)^* \\ = \int_{-\infty}^{+\infty} \boldsymbol{\vartheta}(t - \tau) c(t - \tau)^* dt = \int_{-\infty}^{+\infty} \boldsymbol{\vartheta}(t) c(t)^* dt = \mathbf{w}, \\ \lim_{(N'_1, N'_2) \rightarrow (-\infty, +\infty)} T_s \sum_{n=N'_1}^{N'_2} \boldsymbol{\vartheta}(nT_s - \tau) \boldsymbol{\vartheta}^H(nT_s - \tau) \\ = \int_{-\infty}^{+\infty} \boldsymbol{\vartheta}(t - \tau) \boldsymbol{\vartheta}(t - \tau)^H dt = \int_{-\infty}^{+\infty} \boldsymbol{\vartheta}(t) \boldsymbol{\vartheta}(t)^H dt = \mathbf{W}\end{aligned}$$

with

$$\mathbf{w} = \begin{pmatrix} w_1 \\ w_2 \\ w_3 \end{pmatrix}, \quad \mathbf{W} = \begin{bmatrix} w_1 & w_2^* & w_3^* \\ w_2 & W_{2,2} & \varpi \\ w_3 & \varpi & W_{3,3} \end{bmatrix},$$

where $\varpi = \int_{-\infty}^{+\infty} tc^{(1)}(t) c(t)^* dt$, and $w_1, w_2, W_{2,2}, W_{3,3} \in \mathbb{R}$. From these results, we can write that Φ_η

$$\begin{aligned}\Phi_\eta &= F_s \text{Re} \left\{ \mathbf{Q} \mathbf{W} \mathbf{Q}^H - \frac{(\mathbf{Q} \mathbf{w})(\mathbf{Q} \mathbf{w})^H}{w_1} \right\} \\ &= F_s \begin{bmatrix} W_{3,3} - \frac{|w_3|^2}{w_1} & \omega_c \text{Im} \left\{ \varpi - \frac{w_2 w_3}{w_1} \right\} \\ \omega_c \text{Im} \left\{ \varpi - \frac{w_2 w_3}{w_1} \right\} & \omega_c^2 \left(W_{2,2} - \frac{w_2^2}{w_1} \right) \end{bmatrix},\end{aligned}$$

where from [47] we already have w_1, w_3 and $W_{3,3}$,

$$w_1 = \frac{\mathbf{c}^H \mathbf{c}}{F_s}, \quad w_3 = \mathbf{c}^H \mathbf{\Lambda} \mathbf{c}, \quad W_{3,3} = F_s \mathbf{c}^H \mathbf{V} \mathbf{c},$$

and the remaining terms are computed as

$$\begin{aligned}w_2 &= \int_{-\infty}^{+\infty} c(t) (tc(t))^* dt = \int_{-\frac{F_s}{2}}^{\frac{F_s}{2}} c(f) \left(\frac{j}{2\pi} \frac{dc(f)}{df} \right)^* df \\ &= \frac{1}{F_s^2} \int_{-\frac{1}{2}}^{\frac{1}{2}} \left((\mathbf{D} \mathbf{c})^H \mathbf{v}(f) \right) \left(\mathbf{v}^H(f) \mathbf{c} \right) df \\ &= \frac{1}{F_s^2} \mathbf{c}^H \mathbf{D}^H \left(\int_{-\frac{1}{2}}^{\frac{1}{2}} \mathbf{v}(f) \mathbf{v}^H(f) df \right) \mathbf{c} = \frac{1}{F_s^2} \mathbf{c}^H \mathbf{D} \mathbf{c}, \\ \varpi &= \int_{-\infty}^{+\infty} c^{(1)}(t) (tc(t))^* dt \\ &= \int_{-\frac{F_s}{2}}^{\frac{F_s}{2}} (j2\pi f) c(f) \left(\frac{j}{2\pi} \frac{dc(f)}{df} \right)^* df \\ &= \frac{1}{F_s} \int_{-\frac{1}{2}}^{\frac{1}{2}} (j2\pi f) \left(\mathbf{v}^H(f) \mathbf{c} \right) \left((\mathbf{D} \mathbf{c})^H \mathbf{v}(f) \right) df \\ &= \frac{1}{F_s} \mathbf{c}^H \mathbf{D}^H \left(j2\pi \int_{-\frac{1}{2}}^{\frac{1}{2}} f \mathbf{v}(f) \mathbf{v}^H(f) df \right) \mathbf{c} = \frac{1}{F_s} \mathbf{c}^H \mathbf{D} \mathbf{\Lambda} \mathbf{c}, \\ W_{2,2} &= \int_{-\infty}^{+\infty} |tc(t)|^2 dt = \int_{-\frac{F_s}{2}}^{\frac{F_s}{2}} \left| \frac{j}{2\pi} \frac{dc(f)}{df} \right|^2 df \\ &= \frac{1}{F_s^3} \int_{-\frac{1}{2}}^{\frac{1}{2}} \left| \mathbf{v}^H(f) (\mathbf{D} \mathbf{c}) \right|^2 df \\ &= \frac{1}{F_s^3} \mathbf{c}^H \mathbf{D}^H \left(\int_{-\frac{1}{2}}^{\frac{1}{2}} \mathbf{v}(f) \mathbf{v}^H(f) df \right) \mathbf{D} \mathbf{c} = \frac{1}{F_s^3} \mathbf{c}^H \mathbf{D}^2 \mathbf{c}.\end{aligned}$$

Finally, the other terms in (15b)-(15d) are also computed from \mathbf{w} as follows:

$$\begin{aligned}\text{CRB}_\varphi &= \frac{\sigma_n^2}{2\rho^2} \frac{1}{F_s w_1} + \frac{1}{w_1^2} \\ &\times \left(\frac{\text{Im}\{w_3\} - b\omega_c w_1}{\omega_c w_2} \right)^\top \mathbf{CRB}_\eta \left(\frac{\text{Im}\{w_3\} - b\omega_c w_1}{\omega_c w_2} \right), \\ \mathbf{CRB}_{\eta, \varphi} &= \mathbf{CRB}_\eta \frac{1}{w_1} \left(\frac{\text{Im}\{w_3\} - b\omega_c w_1}{\omega_c w_2} \right), \\ \text{CRB}_\rho &= \frac{\sigma_n^2}{2F_s w_1} + \rho^2 \frac{1}{w_1^2} \left(\frac{\text{Re}\{w_3\}}{0} \right)^\top \mathbf{CRB}_\eta \left(\frac{\text{Re}\{w_3\}}{0} \right).\end{aligned}$$